Oxide Scales Formed on NiTi and NiPtTi Shape Memory Alloys

James L. Smialek, Anita Garg, Richard B. Rogers, and Ronald D. Noebe
Glenn Research Center, Cleveland, Ohio

September 2011

NASA STI Program . . . in Profile

Since its founding, NASA has been dedicated to the advancement of aeronautics and space science. The NASA Scientific and Technical Information (STI) program plays a key part in helping NASA maintain this important role.

The NASA STI Program operates under the auspices of the Agency Chief Information Officer. It collects, organizes, provides for archiving, and disseminates NASA's STI. The NASA STI program provides access to the NASA Aeronautics and Space Database and its public interface, the NASA Technical Reports Server, thus providing one of the largest collections of aeronautical and space science STI in the world. Results are published in both non-NASA channels and by NASA in the NASA STI Report Series, which includes the following report types:

- TECHNICAL PUBLICATION. Reports of completed research or a major significant phase of research that present the results of NASA programs and include extensive data or theoretical analysis. Includes compilations of significant scientific and technical data and information deemed to be of continuing reference value. NASA counterpart of peer-reviewed formal professional papers but has less stringent limitations on manuscript length and extent of graphic presentations.

- TECHNICAL MEMORANDUM. Scientific and technical findings that are preliminary or of specialized interest, e.g., quick release reports, working papers, and bibliographies that contain minimal annotation. Does not contain extensive analysis.

- CONTRACTOR REPORT. Scientific and technical findings by NASA-sponsored contractors and grantees.

- CONFERENCE PUBLICATION. Collected papers from scientific and technical conferences, symposia, seminars, or other meetings sponsored or cosponsored by NASA.

- SPECIAL PUBLICATION. Scientific, technical, or historical information from NASA programs, projects, and missions, often concerned with subjects having substantial public interest.

- TECHNICAL TRANSLATION. English-language translations of foreign scientific and technical material pertinent to NASA's mission.

Specialized services also include creating custom thesauri, building customized databases, organizing and publishing research results.

For more information about the NASA STI program, see the following:

- Access the NASA STI program home page at *http://www.sti.nasa.gov*

- E-mail your question via the Internet to *help@sti.nasa.gov*

- Fax your question to the NASA STI Help Desk at 443–757–5803

- Telephone the NASA STI Help Desk at 443–757–5802

- Write to:
  NASA Center for AeroSpace Information (CASI)
  7115 Standard Drive
  Hanover, MD 21076–1320

Oxide Scales Formed on NiTi and NiPtTi Shape Memory Alloys

James L. Smialek, Anita Garg, Richard B. Rogers, and Ronald D. Noebe
Glenn Research Center, Cleveland, Ohio

National Aeronautics and
Space Administration

Glenn Research Center
Cleveland, Ohio 44135

September 2011

Acknowledgments

The authors thank R. Mattingly for assistance with XRD data acquisition and analysis.

Level of Review: This material has been technically reviewed by technical management.

Available from

NASA Center for Aerospace Information
7115 Standard Drive
Hanover, MD 21076–1320

National Technical Information Service
5301 Shawnee Road
Alexandria, VA 22312

Available electronically at http://www.sti.nasa.gov

Oxide Scales Formed on NiTi and NiPtTi Shape Memory Alloys

James L. Smialek, Anita Garg, Richard B. Rogers, and Ronald D. Noebe
National Aeronautics and Space Administration
Glenn Research Center
Cleveland, Ohio 44135

Abstract

Ni-49Ti and Ni-30Pt-50Ti (at.%) shape memory alloys were oxidized isothermally in air over the temperature range of 500 to 900 °C. The microstructure, composition, and phase content of the scales were studied by SEM, EDS, XRD, and metallography. Extensive plan view SEM/EDS identified various features of intact or spalled scale surfaces. The outer surface of the scale was a relatively pure TiO_2 rutile structure, typified by a distinct highly striated and faceted crystal morphology. Crystal size increased significantly with temperature. Spalled regions exhibited some porosity and less distinct features. More detailed information was obtained by correlation of SEM/EDS studies of 700 °C/100 hr cross-sections with XRD analyses of serial or taper-polishing of plan surfaces. Overall, multiple layers exhibited graded mixtures of NiO, TiO_2, $NiTiO_3$, Ni(Ti) or Pt(Ni,Ti) metal dispersoids, Ni_3Ti or Pt_3Ti depletion zones, and substrate, in that order. The NiTi alloy contained a 3 at.% Fe impurity that appeared in embedded localized Fe-Ti-rich oxides, while the NiPtTi alloy contained a 2 v/o dispersion of TiC that appeared in lower layers. The oxidation kinetics of both alloys (in a previous report) indicated parabolic growth and an activation energy (250 kJ/mole) near those reported in other Ti and NiTi studies. This is generally consistent with TiO_2 existing as the primary scale constituent, as described here.

Introduction

Shape memory alloys (SMA) have been studied and developed for various medical and activating or switching devices that take advantage of a reversible martensitic transformation. While NiTi remains the most widely used composition, the phenomenon is characteristic of many B2 and other ordered intermetallic systems. One distinctive attribute of the NiTi-based nitinol system is the proximity of the transformation range to room temperature. More recently, however, systems with elevated temperature capability have been proposed. For example, ternary alloys based on the Ni-Pt-Ti system have demonstrated transformation temperatures in the range of 300 to 500 °C (Ref. 1). This offers possible applications as turbine engine actuator devices in hot environments. Commonly used hot fabrication techniques (rolling, wire drawing) provide additional motivations to study oxidation behavior. Alternatively, SMA biomaterial implant devices often use pre-oxidized surfaces to facilitate tissue adhesion and bone growth to the TiO_2 scale as well as limit the amount of toxic Ni that may dissolve in vivo fluids. Furthermore, Pt-modified alloys offer improved imaging in atomic number-sensitive CAT scans. Accordingly, the oxidation kinetics have been studied for a Ni-30Pt-50Ti SMA over the temperature range of 500 to 900 °C in a prior companion study (Ref. 2) and compared to those of a commercial Ni-49Ti alloy. Generally, it was found that the kinetics of the NiPtTi alloy were lower than those of the binary by about a factor of 4, but with a similar temperature dependence or activation energy. The purpose of this paper is to augment these findings with corresponding microstructural and phase characterization of the scales using XRD and SEM/EDS, in both plan and transverse cross-section samples.

Prior Literature

NiTi alloy oxidation has been the focus of a number of studies, all finding essentially parabolic kinetics. The kinetic results are summarized in Table 1 (Ref. 2) for an overall temperature range of 450 to 1000 °C and for durations as short as 4 hr and as long as 100 hr. The results are grouped for those having high or low activation energies of 220 to 260 kJ/mole and 130 to 150 kJ/mole, respectively. By comparison, the activation energy of pure Ti is close to 220 kJ/mole and that of pure Ni varies over 110 to 170 kJ/mole, possibly an effect of uncontrolled impurities. While it is tempting to attribute the lower range of NiTi data to some effect of NiO scales, this appears not to be the case as discussed below. At present, the reason for two groupings of activation energy is unresolved.

TABLE 1.—COMPARATIVE ARRHENIUS PARAMETERS FOR Ni-X-Ti OXIDATION KINETICS

$k_p = A \exp(-Q/RT)$

alloy, at.%	A (mg^2/cm^4hr)	A' (g^2/cm^4s)	Q, (kJ/mole)	Temperature (°C)	Duration (hr)	r^2	Reference
Ni30Pt50Ti	1.54×10^{12}	4.29×10^2	**250**	500-900	100	0.98	Smialek (2010)
Ni49Ti	6.39×10^{12}	1.78×10^3	**249**	600-900	100	1.00	Smialek (2010)
Ni50Ti	3.46×10^{12}	9.61×10^2	**259**	750-950	60	0.99	Satow (1974)
Ni50Ti	4.85×10^{10}	13.48	**225**	700-1000	6	0.96	Chu (1996)
Ni50Ti	1.92×10^6	5.33×10^{-4}	136	450-750	4	1.00	Xu (2004)
Ni50Ti	7.31×10^6	2.03×10^{-3}	152	530-650	4	0.96	Vojtêch (2008)
Ni10Cu50Ti	1.61×10^7	4.47×10^{-3}	143	700-925	6	1.00	Lin (2009)
Ti (K)	1.66×10^{10}	4.60	**219**	500-950	N.A.	N.A.	Kofstad (1988)
Ni (K)	7.02×10^3	1.95×10^{-6}	112	600-1200	N.A.	N.A.	Kofstad (1988)
Ni (G)	1.63×10^6	4.52×10^{-4}	167	550-700	6	0.99	Gulbransen (1954)
Ni (P)	1.38×10^6	3.84×10^{-4}	174	815-1370	1-2	1.00	Progar (1964)
Ni (A)	5.22×10^6	1.45×10^{-3}	154	500-800	109	0.98	Atkinson (1982)

In an aggregate picture of the scale make-up, multiple layers are seen to grow with TiO_2 rutile as the outer and predominant scale layer. This gives way to a mixed layer of TiO_2 and $NiTiO_3$. Dispersed Ni(Ti) metal particles and porosity are often observed in the scale. Ti-depletion zones overlie the metal substrate structure, showing Ni_xTi (x = 2,3,4) on top of a TiNi layer having a depressed M_s temperature due to Ti denudation.

Specifically, Satow, Isano, and Honma, in perhaps the first reported oxidation study of NiTi shape memory alloys (1974) (Ref. 3), used a succession of 20 light polishing treatments for layer-by-layer XRD analysis of the scale. They found structures of outer TiO_2, followed by a graded mixture with $NiTiO_3$, a porous Ni(Ti) layer, Ni_3Ti, and finally unaffected TiNi. Chan et al. found primarily TiO_2 scales, with a depletion zone corresponding to "~Ni_2Ti" (Ref. 4). Chu et al. (Ref. 5) found TiO_2 external scales, with metallic Ni(Ti) particles dispersed in an intermediate scale layer, followed by a Ni_3Ti depletion zone. Firstov et al. (Ref. 6) oxidized NiTi for 30 hr at various temperatures. After 30 min, XRD analysis revealed TiO at 300 to 500 °C, TiO_2 at 600 °C, adding some NiO at 700 °C and $NiTiO_3$ at 800 °C. The B19′ martensitic room-temperature phase gave way to the B2 parent phase due to selective Ti oxidation.

With increasing oxidation temperature, Ni_3Ti depletion zones increased while a trace of elemental Ni, very near the gas surface, decreased. Nitinol wires were oxidized for 6 hr at 400 to 1000 °C and characterized (Ref. 7) as external TiO_2 scales, followed by bands of Ni intermixed with TiO_2, and underlying Ni_3Ti, Ni_4Ti depletion layers. Similarly, Vojtěch et al. oxidized nitinol wire for 4 hr at 430 to 650 °C (Ref. 8), resulting in TiO_2 scales, while Xu et al. (Ref. 9) oxidized NiTi for 4 hr at 450 to 750 °C and found primarily TiO_2 scale growth, with Ti-denuded internal oxidation and Ni_3Ti depletion zone layers. Partial spallation occurred after 750 °C oxidation, revealing somewhat of an open or porous interface and individual oxide crystallites. Tian et al. (Refs. 10 and 11) oxidized a high-temperature Ni-30Pd-50Ti at.% shape memory alloy at 900 °C for 46 hr and identified a lenticular, oriented TiO_2-rich outer scale, with an inner porous layer containing $NiTiO_3$ and Ti_4Pd_2O. Below the scale, a 250 µm Ti depletion zone in the substrate was found to cause a dramatic rise in hardness. These alloys oxidized somewhat slower than binary NiTi and pure Ti. Most recently Lin and Wu oxidized another ternary alloy, Ni10Cu50Ti, at 700 to 1000 °C for 6 hr (Ref. 12). They found highly-layered structures of external Cu_2O, $TiO_2 + TiNiO_3$, $TiO_2+Ni(ss)$ and $(Ni,Cu)_3Ti$ depletion layers.

The following, then, is an attempt to characterize the various scale phases and layers that form on the subject Ni-49Ti and Ni-30Pt-50Ti shape memory alloys that were reported in an earlier study of the 500 to 900 °C oxidation kinetics (Refs. 2 and 13). While XRD was used to identify phases, a wide variety of scale microstructural features were detailed by SEM/EDS. Most samples were studied in plan of the oxidized surface, but 700 °C samples were characterized in more detail by cross-section microstructure and serial-section XRD.

Materials and Experimental Procedure

A conventional Nitinol shape memory alloy was obtained commercially from Johnson Matthey Inc., in the form of 0.125 in. (3.18 mm) rolled plate which was then surface ground to 0.100 in. (2.54 mm) and electro-discharge machining (EDM) sectioned into 3/4 by 3/4 in. (1.9 by 1.9 cm) coupons. Chemical analysis of the Ni-49Ti alloy (subsequently called Ni49Ti), performed by ICP, yielded Ni-49.3Ti-3.2Fe at.%. The Ni-30Pt-50Ti alloy (subsequently called Ni-30Pt-50Ti) was produced in our laboratory by vacuum induction melting in a graphite crucible, cast into a 1 in. diameter by 4 in. (2.54 cm diameter by 10.2 cm) long cylinder, and forged to 0.42 in. (1.07 cm), under a 1093 °C preheat. The plate was EDM sectioned into 0.100 in. (2.54 mm) thick by 0.6 by 0.6 in. (1.5 by 1.5 cm) coupons. The primary alloy phase at room temperature was the B19 ordered orthorhombic martensite, with an unintentional 2.1 vol% TiC dispersed particulate phase in the Ni-30Pt-50Ti material and an overall chemistry of 20.10 Ni, 49.66 Ti, 29.1 Pt, 0.85 C, 0.2 O, 0.06 N, and 0.02 Fe atomic percent. Oxidation coupons were polished to a 600 grit finish with SiC emery paper and ultrasonically cleaned in detergent, then ethyl alcohol.

The samples were oxidized in dried, bottled air, flowing at 100 cm^3/min., at 500, 600, 700, and 800 °C for 100 hr, and at 900 °C for 10 hr in a Cahn 1000 thermogravimetric analysis (TGA) electrobalance using an alumina tube and resistance furnace. The detailed treatment of the TGA kinetic data was discussed in the companion paper (Ref. 2).

The surface of oxidized coupons were characterized by x-ray diffraction (XRD). Select 700 °C samples were also examined by serial-sectioning the binary Ni49Ti alloy or by microfocus XRD by low angle (≤1°) taper-section polishing of the ternary Ni-30Pt-50Ti alloy. Here the oxidized surface was carefully polished with 600 grit emery paper, finishing with 4000. Periodically the sample weight was recorded and the sample was submitted for XRD analyses. The relative amounts of phases were estimated from the diffracted intensities of each phase using a commercial software program.

FEG-SEM/EDS scanning electron microscopy was performed on oxidized surfaces using a conductive carbon coating and a typical accelerating voltage of 15 kV. Scale feature chemistry was characterized by EDS using a windowless detector. The primary (and secondary satellite) peaks observed in this study follow in order of energy level as C K_α, (Ti L_1, Ti L_α) O K_α, Ni L_1, Ni L_α, (Pt M_2) Pt M_α, (Pt M_γ), Ti K_α, (Ti K_β), Fe K_α, (Fe K_β), Ni K_α, (Ni K_β), and (Pt L_1, Pt L_α) over the energy range of about 0.2 to 10.0 kev.

Results

The as-received microstructure of the Ni-30Pt-50Ti alloy is shown in Figure 1, as a dispersion of TiC in a matrix of heavily twinned martensite. A cross-section of the 500 °C oxidized sample reveals a thin, ~0.2 μm, Ti-O rich surface scale. The corresponding EDS results, Figure 2, support this chemistry, allowing for beam overlap at features smaller than the electron interaction volume, at ~1 μm^3. (Here and afterwards, the abscissa refers to relative intensity in arbitrary units while the ordinate is the standard electron energy in keV).
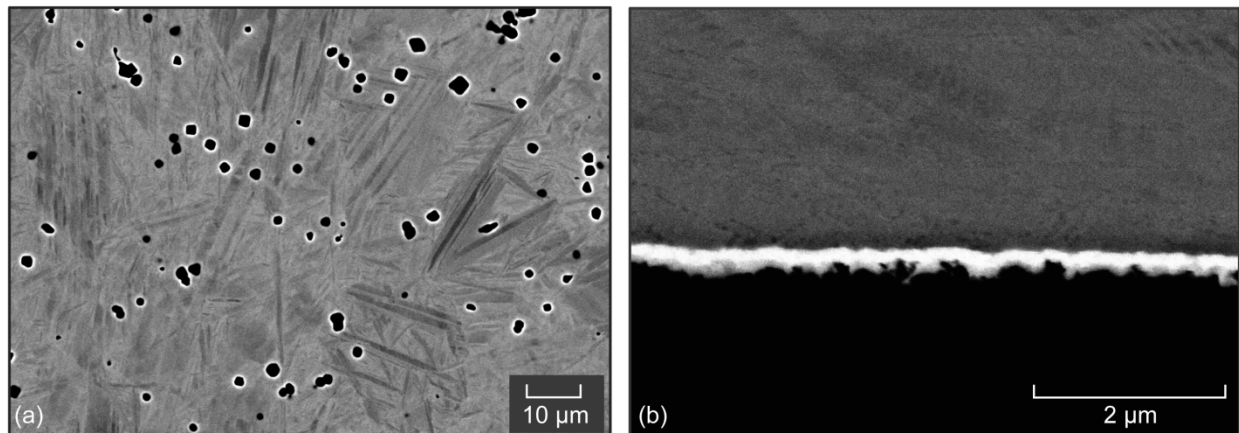
Figure 1.—Cross-section microstructure of Ni30Pt50Ti (a) as-received and (b) 500 °C, 100 hr oxidation.
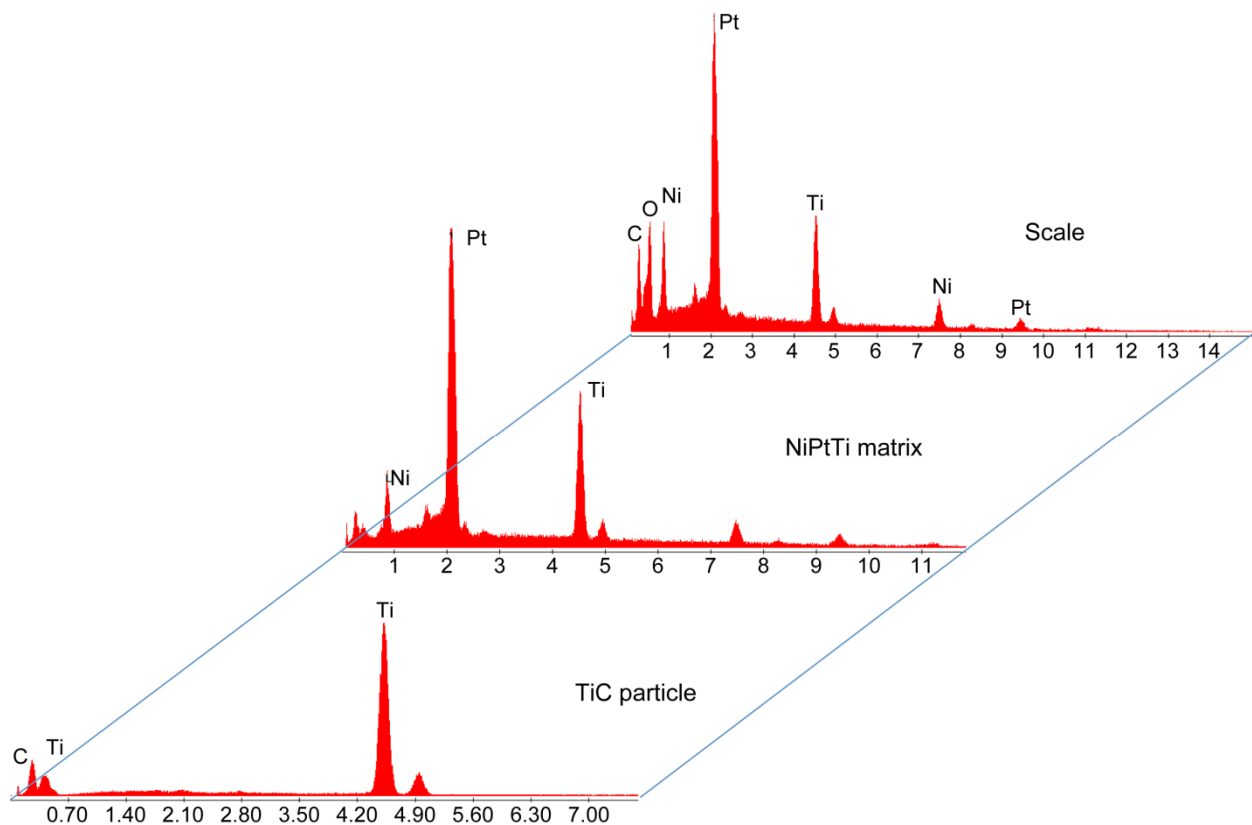
Figure 2.—SEM/EDS identification of dark TiC particles, Ni30Pt50Ti matrix, and thin scale in Figure 1.

Spalling after cool-down was observed for some samples, shown by surface macrographs and weight change (Ref. 2). The relative amount of oxide weight loss on cool-down was compared to the final oxygen weight gain before cool-down. The relative amount of spalling was estimated, up to ~70 percent for Ni49Ti above 700 °C and up to ~55 percent for Ni-30Pt-50Ti above 800 °C, correcting for stoichiometry and assuming primarily TiO_2 scales. Thus, it is recognized that surface characterizations discussed below will sometimes correspond to inner scale layers exposed due to spalling.

Overview of XRD Phase Analysis

A summary of the primary scale and metal phases identified by XRD of the oxidized surfaces is shown in Table 2. Representative patterns demonstrating these results are presented in Figures 3 and 4 for Ni49Ti and Ni-30Pt-50Ti after various exposures. The as-received room temperature metal phases were the cubic B2 NiTi "austenite" and the orthorhombic B19 Pt(Ni)Ti martensite structures. For both alloys, TiO_2 rutile was the predominant surface scale. The anatase phase may have been present, but only in very small amounts at low temperatures (500 and 600 °C). The $NiTiO_3$ nickel titanate phase appeared on both alloys and was more prevalent for the Ni-30Pt-50Ti alloy. NiO was not a major scale phase, but appeared with preferred orientation on the Ni-30Pt-50Ti alloy.

TABLE 2.—XRD PHASE SUMMARY FOR OXIDIZED Ni(Pt)Ni SHAPE MEMORY ALLOYS
a) Ni49Ti; b) Ni-30Pt-50Ti

a) Ni49Ti

T (°C)	t (h)	scale	B2 NiTi	D0$_{24}$ Ni$_3$Ti	A1 Ni		rutile TiO$_2$	anatase TiO$_2$	NiTiO$_3$	NiO
		as-received	S							
500	100	surface	S	W			W	V.W.	M	
600	100	surface	M	M			S	W	W	
700	100	surface					S		V.W.	
700	100	spall					S		W	
800	100	surface					S		V.W.	
800	100	spall					S			
900	10	surface			S		S		W	V.W.

b) Ni30Pt50Ti

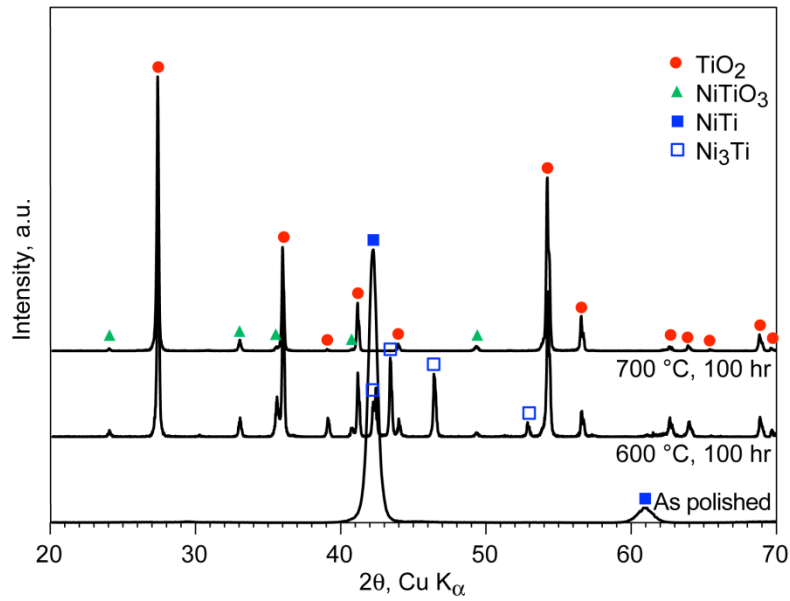| T (°C)	t (h)	scale	B19 Pt(Ni)Ti	L1$_2$ Pt$_3$Ti	L1$_0$ NiPt	A1 Pt(Ni)	rutile TiO$_2$	anatase TiO$_2$	NiTiO$_3$	NiO
		as-received	S							
500	100	surface	S	M	M		M	V.W.		
600	100	surface	W	S	V.W.	S	M	W?		
700	100	surface		W?		S	S		S	M
800	100	surface		W?		M	S		W	
900	10	surface				M	S		V.W.	

Figure 3.—Representative diffractometer scans of oxidized NiTi surface before and after 100 hr oxidation at 600 and 700 °C showing patterns for B2 NiTi substrate, Ni_3Ti depletion zone, and TiO_2 and $NiTiO_3$ scale phases.
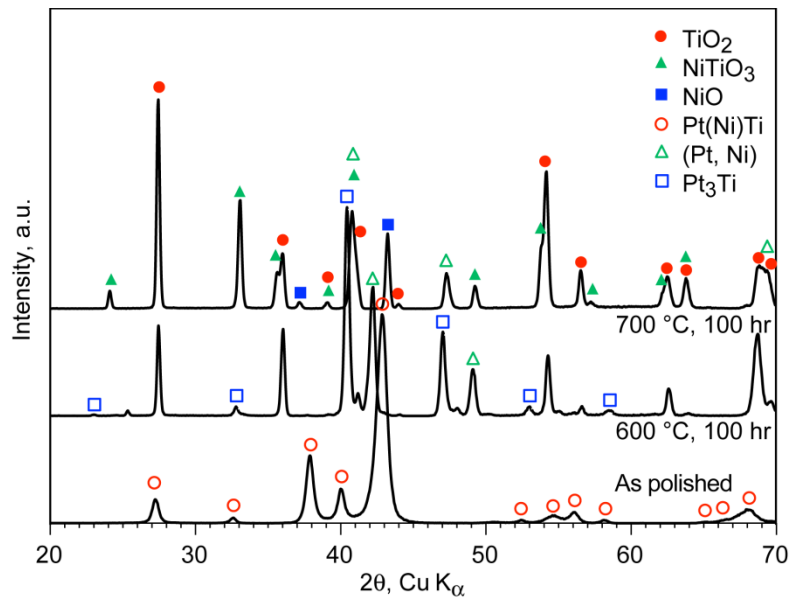
Figure 4.—Representative diffractometer scans of oxidized Ni(Pt)Ti surface before and after 100 hr oxidation at 600 and 700 °C showing patterns for B19 Pt(Ni)Ti substrate, Pt(Ni) + Pt_3Ti depletion zone, and TiO_2 and $NiTiO_3$ scale phases.

As already mentioned, cooling from oxidation at the higher temperatures produced massive spalling. Thus the true outer layer could not always be represented by a surface diffractometer scan. For Ni49Ti it was possible to collect some spalled material from the 700 and 800 °C scales for analyses; these confirmed essentially the same scale phases as the surface scans (Table 2). The metal phases identified after oxidation were B2 NiTi, $L1_2$ Ni_3Ti, and A1 FCC Ni for the Ni49Ti alloy and B19 Pt(Ni)Ti, Pt_3Ti, $L1_0$ NiPt, FCC Pt(Ni) and a $D0_{19}$ phase for the Ni-30Pt-50Ti alloy.

Serial Polishing of Ni49Ti, Taper Section of Ni-30Pt-50Ti, and SEM Cross-Sections After 700 °C Oxidation

Ni49Ti XRD Results

The cross-sectional microstructure of a duplicate Ni49Ti sample oxidized at 700 °C for 100 hr is shown in Figure 5. The total scale and metal depletion zones are on the order of 30 and 17 μm, respectively. Multiple layers are clearly delineated. Some representative diffractometer scans highlighting the major phases are shown for the 700 °C samples in Figure 6. With no polishing (P0), TiO_2, and $NiTiO_3$ are seen as the major surface phases. After slight polishing (P2), the relative amount of $NiTiO_3$ increases. Finally, near the substrate layer (P7), metallic Ni and Ni_3Ti are revealed. More detailed data showing the gradation of phase mass content (estimated) with surface polishing is listed in Table 3 and Figure 7 for the 700 °C samples. It should be noted in these analyses that the immediate underlying layers will contribute somewhat to the diffracted intensity because of significant penetration depths (many microns) in conventional XRD analyses. TiO_2 rutile was the major oxide phase throughout the scale layers. Also, a small amount of $NiTiO_3$ was mixed with TiO_2 in the outer layers, reaching a maximum after about
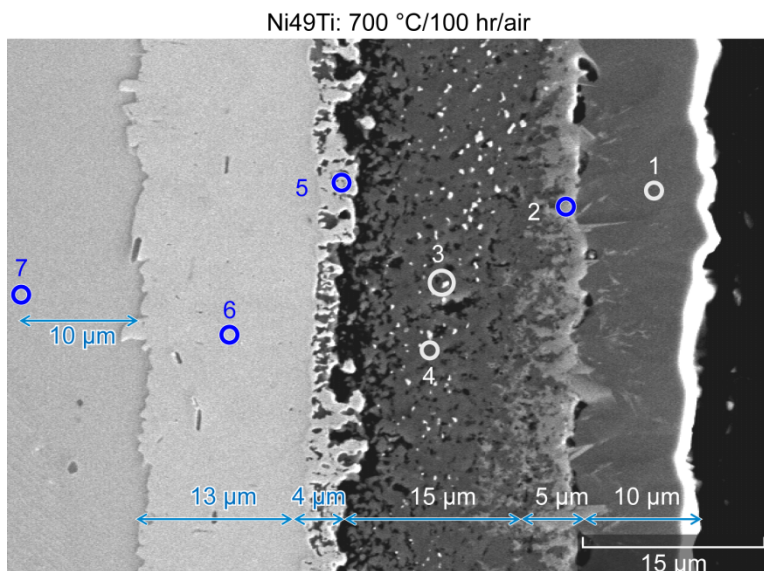
Ni49Ti: 700 °C/100 hr/air

Figure 5.—Cross-section microstructure of multilayer scale on Ni49Ti after 100 hr 700 °C oxidation showing dispersed metal particles and thick depletion zone.
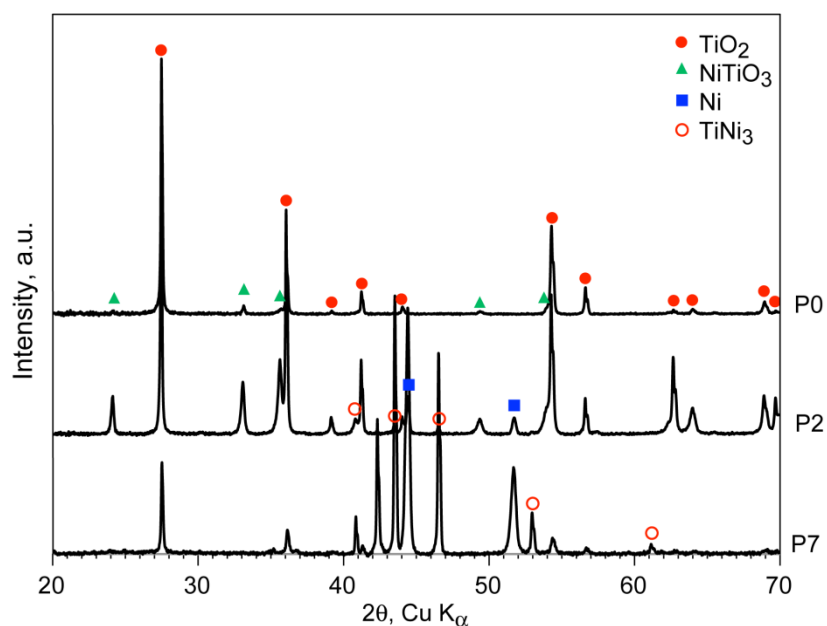
Figure 6.—Representative diffractometer scans of oxidized NiTi surface after 100 hr oxidation at 700 °C. Patterns for sequential serial-polishing layers show external TiO_2 and $NiTiO_3$ scale phases, then Ni and Ni_3Ti depletion zone metal phases. (From Table 3, P0 refers to no polishing, P2 slight polishing, and P7 final polishing near the substrate).

TABLE 3.—SEMI-QUANTITATIVE ESTIMATE OF PHASES IN POLISHED SERIAL SECTIONS
Ni49Ti, OXIDIZED AT 700 °C, 100 HR

	$\Delta W/A$ mg/cm^2	TiO_2	$NiTiO_3$	Ni	Ni_3Ti	NiTi	Fe_3O_4
P0	0.00	95	5				
P1	0.23	89	9	2	T	T	T
P2	2.22	66	19	4	1		4
P3	2.98	78	13	7	2		
P4	3.79	80	7	10	3		
P5	6.13	78		14	8		
P6	8.20	54		22	23	1	
P7	9.35	13		31	56		
P7, edge	9.35	4		14	82		
TiO_2 scale	10.67						

T = trace
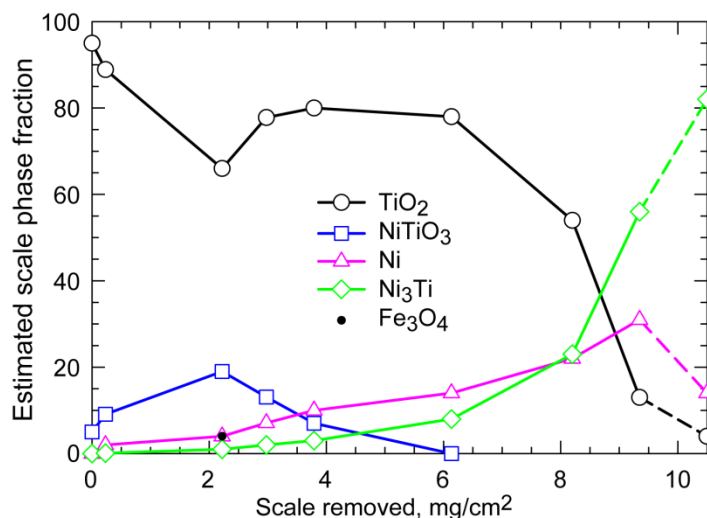
Figure 7.—Semi-quantitative trends in scale and depletion zone phase content: serial section XRD scans of Ni49Ti after 100 hr 700 °C oxidation. TiO_2 major scale phase, with lesser $NiTiO_3$; metallic Ni and Ni_3Ti increasing at inner scale layer.

2 mg/cm^2 scale removal, disappearing at 6 mg/cm^2 removal. A small amount of Fe-rich oxide is identified, primarily at this maximum, arising from the Fe impurity in this alloy. Interestingly, a considerable amount of metallic Ni is seen to be increasing with depth throughout the scale. This Ni phase and the TiO_2 scale finally diminish as the metallic Ni_3Ti depletion zone is encountered. Most of the scale was removed during this sequence, as implied by the 9 mg/cm^2 mass removal approaching the estimated amount of 11 mg/cm^2 scale present. However, in this series, the underlying NiTi base alloy was never exposed. (Note: The final sequence of layer removal by polishing (dashed lines for P7) was graphed at an increased depth for clarity, corresponding to a tapered-edge scan).

Cross-Sectional SEM/EDS of Ni49Ti

For reference, the various features highlighted below are matched with corresponding XRD phase analyses of the serial sections in Table 4. The 15 kV EDS spectra corresponding to the outer layer in Figure 5 (point #1 and spectra #1) is a relatively featureless and pure TiO_2, Figure 8. (Note the common overlap between the O K_α and Ti L_1, Ti L_α lines. It is observed that these lines are not necessarily increased when there is a strong Ti K_α line. Therefore it assumed that these lines primarily reflect the contribution of O K_α). Carbon is commonly present in EDS spectra because of the conductive carbon coating on all samples, but primarily at 15 kV operating voltages. At 10 µm down in Figure 5, some porosity and ingrown Fe-rich oxide platelets or needles are noted (point #2 in Fig. 5), presumably associated with the 3 percent Fe impurity of this alloy. The corresponding EDS spectra (point #2 in Fig. 8) reveals strong Fe and O peaks and moderate Ti and Ni. The 15 µm layer below the needles (#4 in Figs. 5 and 8) is again basically TiO_2, but with a considerable dispersion of submicron Ni-rich particles (point #3 in Figs. 5 and 8), probably metallic. (This oxide spectra in Fig. 8 is distinguished by the low O peak). As with many other instances to follow, there is contribution to small particle (≤1 µm) EDS analyses from the surrounding areas.

TABLE 4.—SERIAL AND TAPER SECTION XRD WITH CORRESPONDING SEM IMAGE AND EDS SPECTRA

a) Ni49Ti		(SEM figure 5)	b) Ni30Pt50Ti		(SEM figures 10,16)
XRD phase	EDS figures:	SEM point/EDS#	XRD phase	EDS figures:	SEM point/EDS#
TiO_2	8	1,4	TiO_2	13,14	3,5
$NiTiO_3$	8	2	NiO	13	1
Fe_3O_4	8	2	$NiTiO_3$	13	2
Ni	8	3	Pt(Ni)	14	4,6
Ni_3Ti	9	5,6	$(Pt,Ni)_3Ti$	15	7
(NiTi)	9	7,8	Pt_3Ti	15	8
			Pt(Ni)Ti	17	11 (LGM)
			DO_{19}	17	10 (WGB)
			TiC	15,17	9,12 (BP)

LGM = light grain matrix
WGB = white grain boundary
BP = black phase
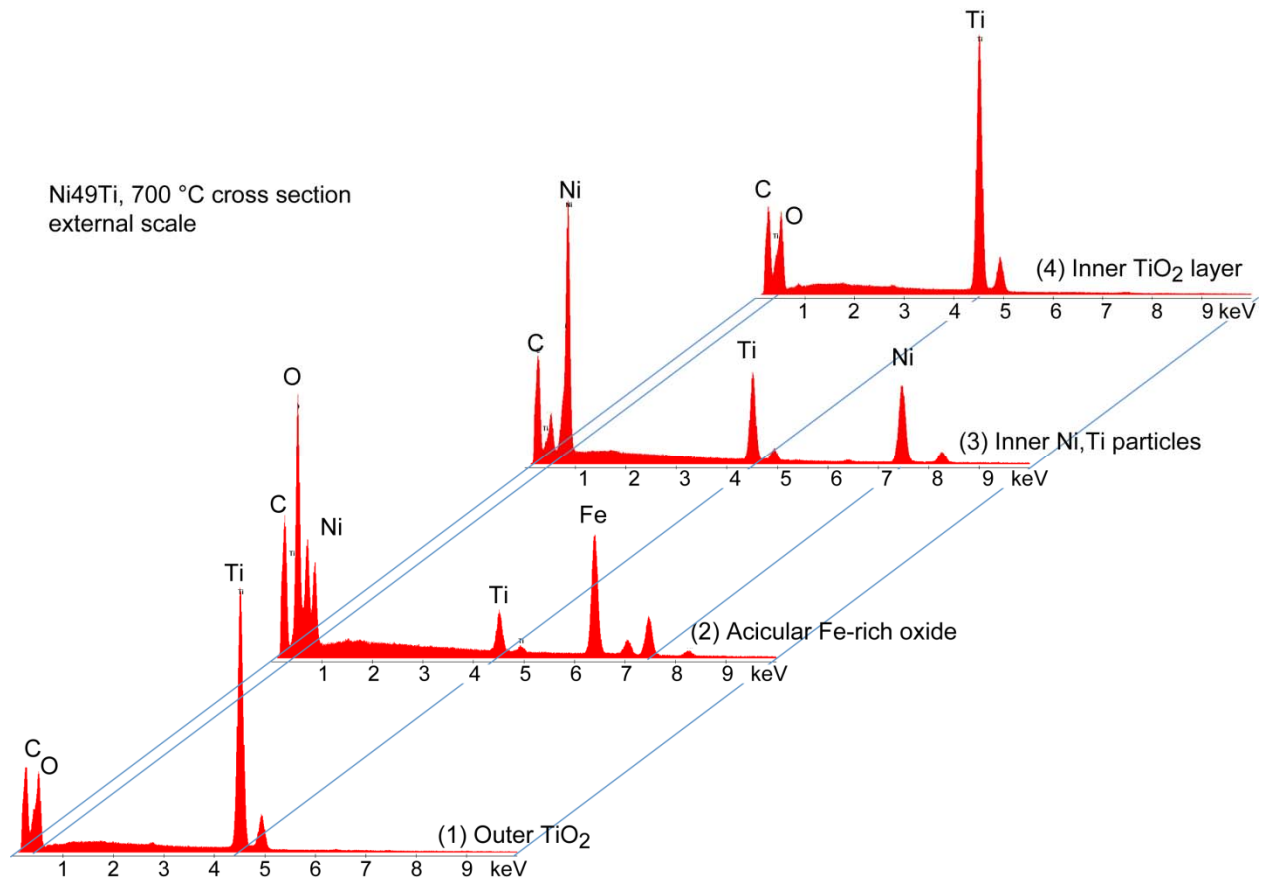
Figure 8.—SEM/EDS spectra corresponding to scale features 1 to 4 from Figure 5 (Ni49Ti after 100 hr 700 °C oxidation).
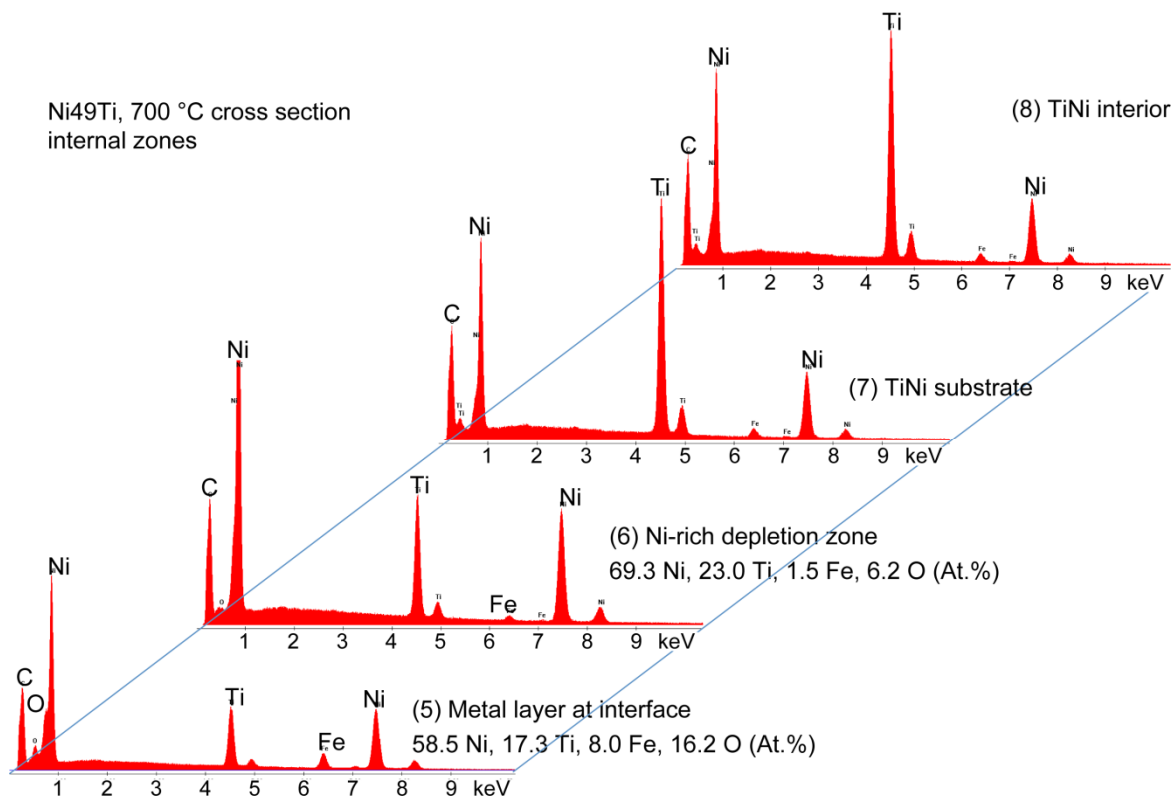
Figure 9.—SEM/EDS spectra corresponding to metallic subscale features 5 to 8 from Figure 5 (Ni49Ti after 100 hr 700 °C oxidation).

Porosity is also increasing at inner regions of this layer, especially at the interface with the next lower layer. Here, the first connected metal phases appear, over a 4 µm thickness, as finger-like protrusions (#5 in Fig. 5), with porosity at the scale interface. The associated spectra in Figure 9 (#5) is similar to that of the Ni(Ti) particles (point #3 in Fig. 8), and the composition, corrected from EDS intensities, is near that of Ni_3Ti, with 8 percent Fe and a substantial amount of oxygen (16 percent). These are connected to the dense depletion zone (#6 in Figs. 5 and 9), also presumably Ni_3Ti, but with less Fe (1.5 percent) and oxygen (6 percent) than the protrusions. Finally, at a level ~10 µm beneath this depletion zone, (#7 in Figs. 5 and 9), the composition of the substrate appears to be essentially the same as the interior of the sample, (#8 in Fig. 9).

The correspondences between serial polishing XRD phase analysis and specific cross-sectional SEM/EDS features are listed in Table 4. In combination, they indicate primarily a duplex TiO_2 scale throughout, with indistinguishable $NiTiO_3$ in the outer layer, interfacial Fe_3O_4 needles above the inner layer, metallic Ni particles dispersed within the inner layer, followed by Ni_3Ti fingers and depletion zone before reaching the NiTi substrate.

Ni-30Pt-50Ti XRD Results

A cross section of the Ni-30Pt-50Ti sample oxidized at 700 °C for 100 hr is shown in Figure 10. First, it appears that a 3-µm outer layer is missing by polishing pullout. The remaining scale can be described as about 5 µm of a three-phase zone and about 8 µm of an inner layer dispersed with numerous metal particles. This yields a total scale of about 16 µm. It is about half the scale formed on Ni49Ti at the corresponding conditions, as expected for the overall k_p ratio of Ni-30Pt-50Ti to Ni49Ti of 1/4. Diffractometer scans of the layers in plan view were primarily resolved by a taper section, as one early polishing step had removed the entire scale at one corner of the coupon, precluding a controlled serial-
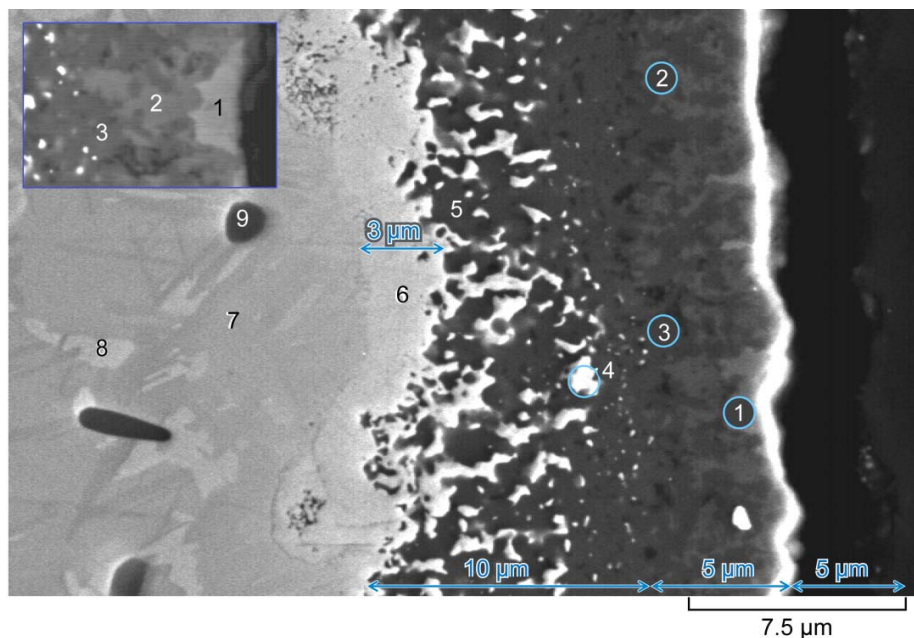
Figure 10.—Cross-section microstructure of multilayer scale on Ni30Pt50Ti after 100 hr 700 °C oxidation showing mottled scale, dispersed metal, and diffuse depletion zone.

sectioning study. Instead the microfocus capability of a special diffractometer was used to locate the beam within a series of distinct adjacent bands, referred to later as "A" to "E", each a few mm wide, across the surface (not shown), and apply to different layers beneath the surface as revealed by taper polishing. Various polishing sequences (0, 1, 2, 3) are also identified by the numerical suffix, for example A0, A1, A2, A3, B2, B3, etc. for the original 5 bands, then F4 and F5 for polishing below the scale to the substrate as defined in Table 5. Some representative diffractometer scans highlighting the major phases are shown in Figure 11 for successive bands A0, D2, and F5, corresponding to increasing depth below the surface. Again, TiO_2 was the primary outer scale phase, with noticeable $NiTiO_3$ and NiO with preferred orientation. Deeper into the depletion zones, strong peaks for Pt_3Ti were found with some Pt(Ni). Finally the unaffected substrate (F), deep into the sample, showed primarily a $D0_{19}$ ordered orthorhombic phase (cf. Ni_3Sn and Ti_3Al structures) and B19 Pt(Ni)Ti.

Semi-quantitative XRD mass % results for scale phases of successive zones, through the 700 °C scale on the NiPtTi alloy, are also listed in Table 5. By inspection, it is apparent that the unpolished and 1st polishing scans, A0 and A1, are nearly identical and the values of the five "A" to "E" bands identified in the 2nd and 3rd polishing series are fairly similar. The values for similar bands were thus averaged and presented in Figure 12(a) for primary scale phases and Figure 12(b) for primary metallic phases, to provide a semiquantitative overview of the trend in surface phases with depth. TiO_2 rutile was the predominant outer scale phase, at least through band "C", with a noticeable concentration of $NiTiO_3$. The latter phase was localized in the outer layer and decreased in the inner bands. A small amount of NiO was detected in the outermost layers. When presenting the metallic phases, Figure 12(b), it is apparent that some metallic FCC Pt(Ni) increases from 10 percent in the outer layer to about 40 percent at band "C". In band "D", Pt_3Ti takes over as a primary phase, with Pt(Ni) and Pt(Ni)Ti phases. Band "C" can thus be seen as a transition zone to the underlying metallic depletion zones. The last band, believed to be unaffected substrate (E3, F4, and F5 in Table 5), consists of B19 Pt(Ni)Ti, hexagonal phase, and the TiC dispersion. The hexagonal phase (c = 5.496Å, a = 4.500 Å) appears to belong to space group P63/mmc (194) with the Ni_3Sn prototype structure ($D0_{19}$). It is isostructural with an $Mn_{12}Pt_4N$ phase and has a good lattice parameter match, but little relation to this composition. To our knowledge, it has not been previously identified in the NiPtTi system. This phase will be referred to subsequently as "$D0_{19}$".
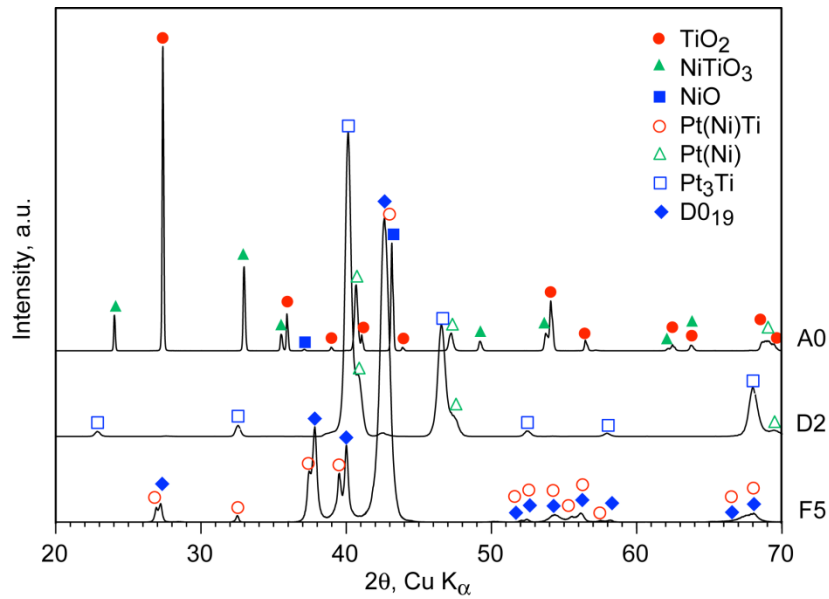
Figure 11.—Representative diffractometer scans of oxidized Ni-30Pt-50Ti surface after 100 hr oxidation at 700 °C. Sequential tapered polishing bands show patterns for external TiO_2 and $NiTiO_3$ scale phases, then $Pt(Ni)$ and Pt_3Ti depletion zone phases, and finally $Pt(Ni)Ti$ and $D0_{19}$ substrate metal phases. (From Table 5, A0 refers to no polishing, D2 is the fourth band in second polishing sequence, and F5 for final polishing to substrate).
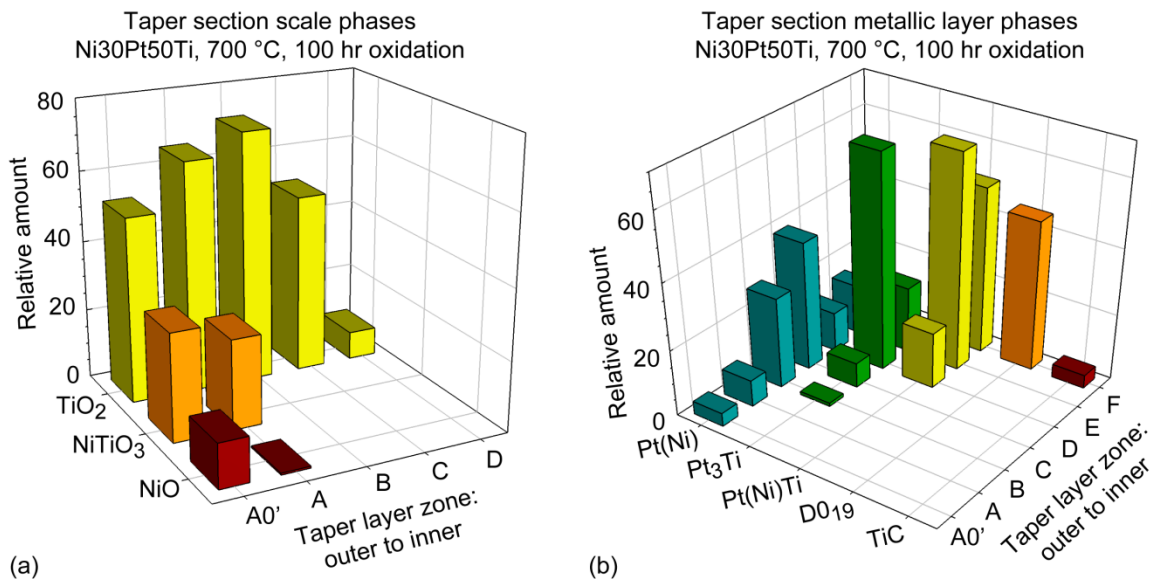

Figure 12.—Trends in semi-quantitative (a) scale and (b) depletion zone phase content from XRD scans of taper section bands (Ni30Pt50Ti after 100 hr, 700 °C oxidation).

TABLE 5.—SEMI-QUANTITATIVE ESTIMATE OF PHASES IN TAPER SECTION BANDS
Ni-30PT-50Ti, OXIDIZED AT 700 °C, 100 HR

layer, zone	ΔW/A mg/cm^2	TiO$_2$	NiO	NiTiO$_3$	Pt(Ni)	Pt$_3$Ti	PtTi	DO$_{19}$	TiC
A0	0.00	49	14	32	4				
A1	0.04	56	11	29	4				
A2	1.58	64	2	27	7				
B2	1.58	75			23	2			
C2	1.58	51			40	9			
D2	1.58	10			24	64	6		
E2	1.58				15	20	65		
A3	2.24	67	0	24	9				
B3	2.24	68			32	1			
C3	2.24	51			38	11			
D3	2.24	6				66	28		
E3	2.24						58	42	
F4	12.76						52	43	5
F5	59.65						49	48	3
TiO$_2$ scale	3.79								

Cross-Sectional SEM of Ni-30Pt-50Ti

For reference, the various other features highlighted below are matched with corresponding XRD phase analyses of the taper section in Table 4. The EDS spectra in Figures 13 to 15 correspond to various points labeled in the scale cross section of Figure 10. The spectra of Figure 13 indicate a small amount of NiO, more NiTiO$_3$, and the remainder being TiO$_2$ for points #1, 2, and 3 in Figure 10, i.e., the intermingled light, gray, and dark scale phases, respectively, with an enlarged example shown in the inset. Spectra from the next layer, Figure 14, indicate basically a dark TiO$_2$ matrix (point #5), with bright, Pt-rich dispersed submicron metal particles and coarser, elongated fingers (point #4). The high carbon peak here suggests some contribution from TiC particles, not readily distinguished. The Pt fingers are then ultimately connected to a continuous, 3-µm, nearly pure, Pt metal depletion zone (point #6). Spectra for the diffusion affected substrate, shown in Figure 15, shows two similar Pt(Ti)-rich gray (point #7) and light (point #8) metal regions, with dark Ti(Pt)-C dispersed particles (point #9). Finally, the interior of the sample, shown in Figure 16, displays a grain boundary necklace of a white phase with a light gray grain interior. These both produce similar Pt(Ti) EDS spectra, Figure 17, and very low Ni content in the white phase. The very dark particles reflect the dispersed TiC phase identified in the as-received material, but again with only a moderately enhanced carbon peak relative to the other spectra. There is also a dark gray Widmanstatten-type morphology that appears to be associated with the bright grain boundary phase. This gray acicular phase was not analyzed.
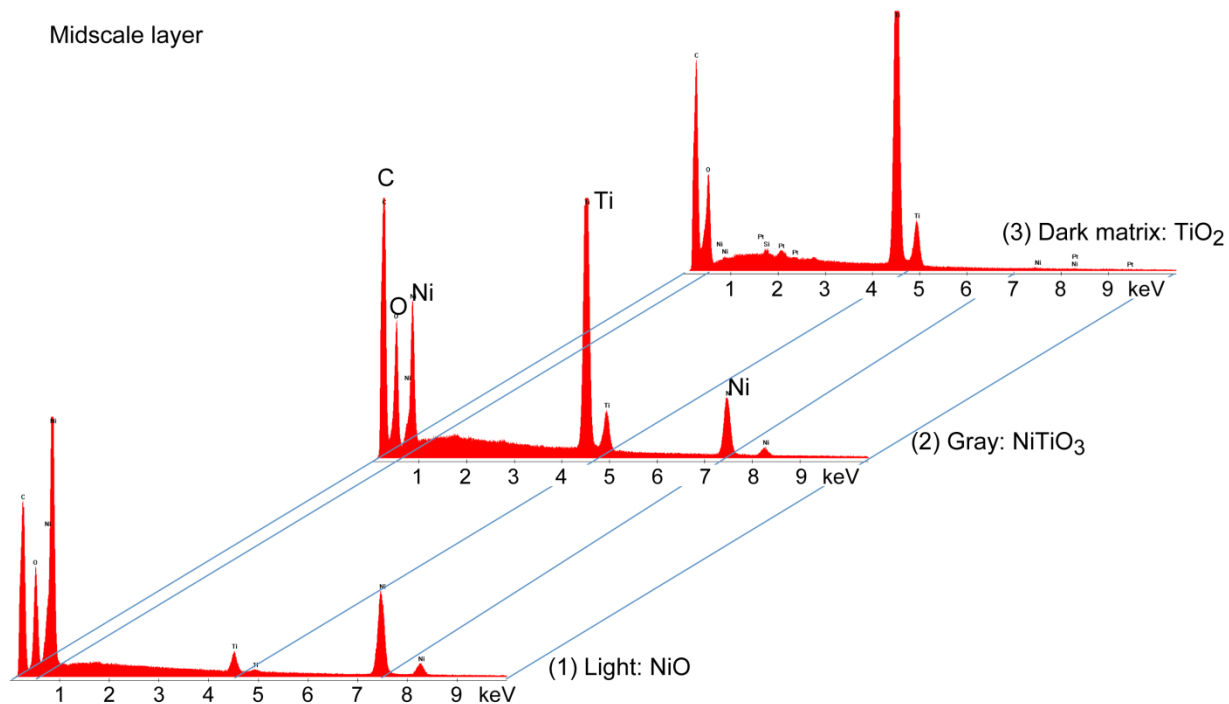
Midscale layer

(1) Light: NiO

(2) Gray: NiTiO$_3$

(3) Dark matrix: TiO$_2$

Figure 13.—SEM/EDS spectra corresponding to outer scale features 1 to 3 from Figure 10 (Ni30Pt50Ti after 100 hr 700 °C oxidation).

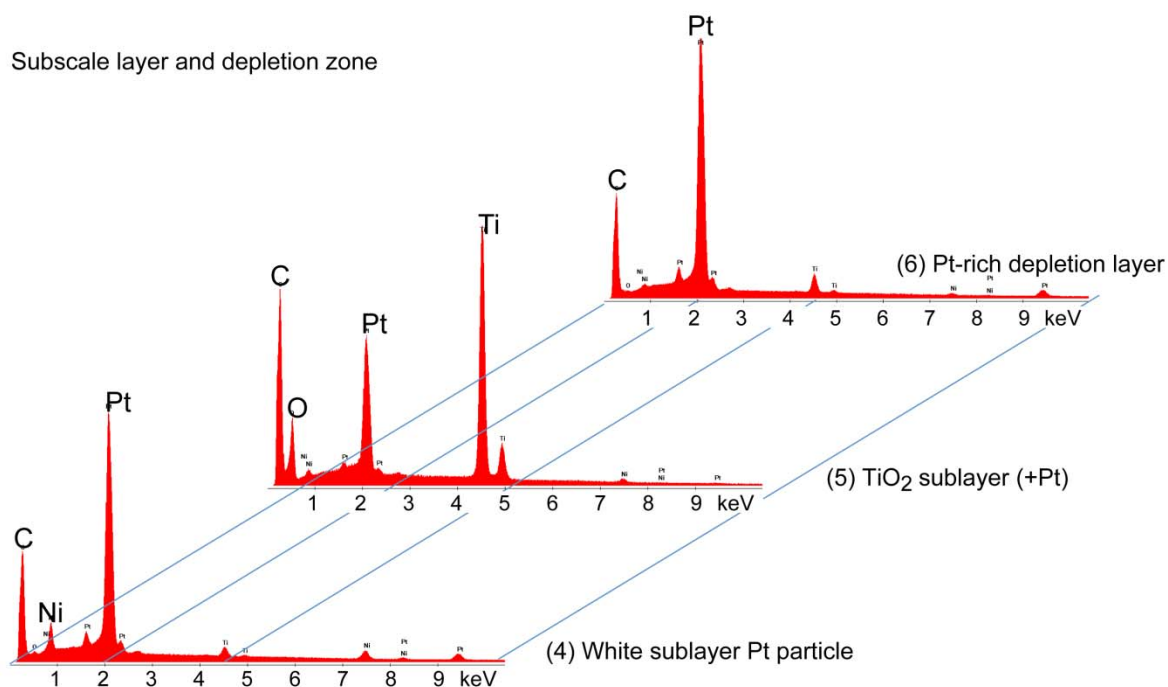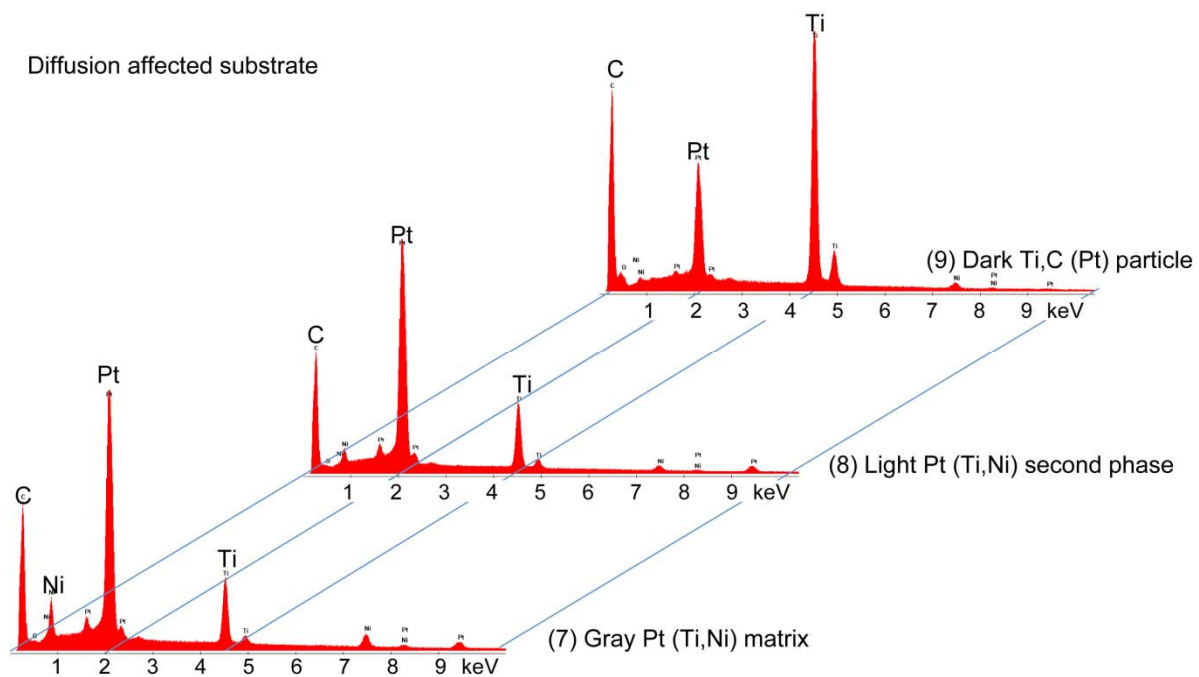Subscale layer and depletion zone

(4) White sublayer Pt particle

(5) TiO$_2$ sublayer (+Pt)

(6) Pt-rich depletion layer

Figure 14.—SEM/EDS spectra corresponding to subscale features 4 to 6 from Figure 10 (Ni30Pt50Ti after 100 hr 700 °C oxidation).

Diffusion affected substrate

Figure 15.—SEM/EDS spectra corresponding to near substrate features 7 to 9 from Figure 10 (Ni30Pt50Ti after 100 hr 700 °C oxidation).

Alloy interior
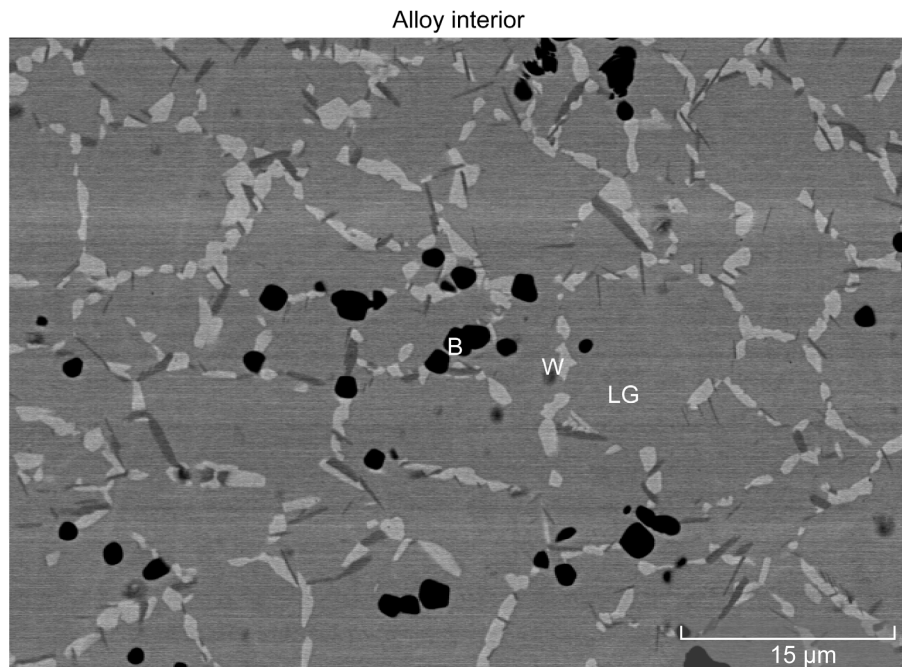
Figure 16.—Grain boundary-decomposition phase in unaffected substrate midsection.
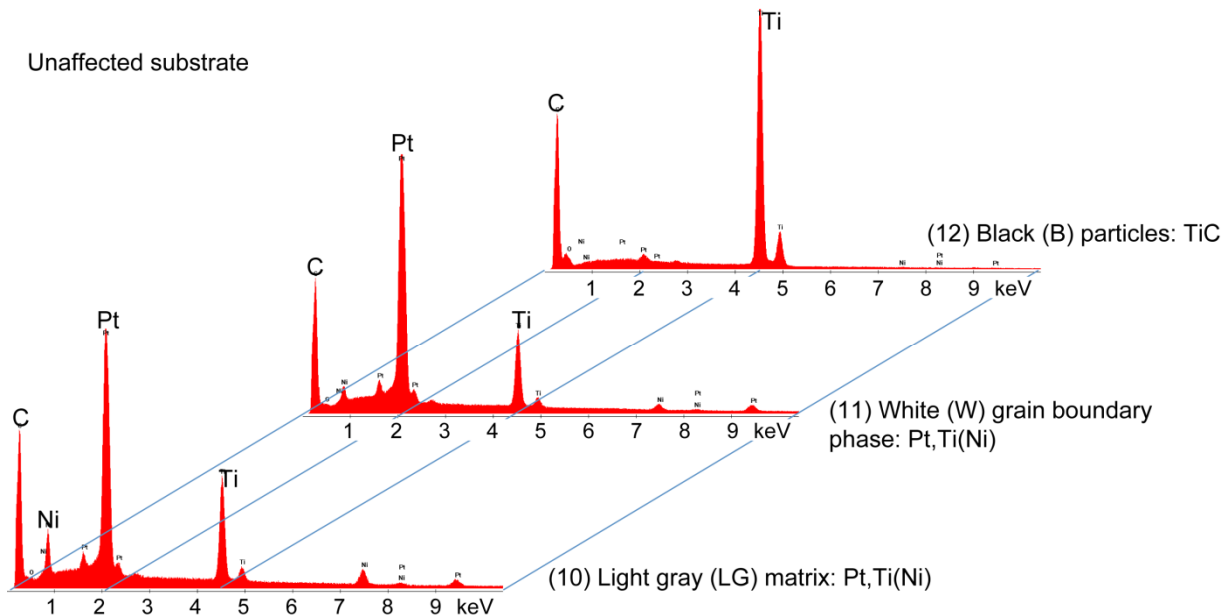
Figure 17.—SEM/EDS spectra corresponding to subscale features 10 to 12 (LG grain center, W grain boundary, B particle) from Figure 16 (Ni30Pt50Ti after 100 hr, 700 °C oxidation).

Plan View of Surface Scales

Ni49Ti

Given this overview, we now proceed to the characterization of the various detailed features that present themselves at the surface in plan view. An overview of the surface structure for scales formed on Ni49Ti by oxidation at 600 to 900 °C is presented in Figure 18, showing the strong effect of oxidation temperature. Here angular, often striated and faceted crystals were easily discerned for the 600 to 800 °C samples, with a grain size clearly increasing with temperature. These are hallmark characteristics of outward TiO_2 rutile scale growth. For the sake of clarity, these are shown at higher magnification for 600 °C oxidation, Figure 19, along with a relatively clean Ti, O spectra. Unfortunately, at 900 °C, spalling was so prevalent that no area of intact scale surface could be located, and the exact scale-gas surface is not represented in Figure 18.

Thus a feature common to the scales formed above 700 °C is the appearance of fracture ledges and plateaus due to complex spall patterns. An example of these is shown in Figures 20(a) and (b) for Ni-49Ti oxidized at 700 °C for 100 hr. Here three layers and two fracture ledges are revealed, with the top layer representing the gas surface. EDS spectra for the top fracture ledge indicates pure TiO_2 (Fig. 21(a)). Within this ledge, some brighter particles yield a Ni-Ti-O rich chemistry, probably indicating $NiTiO_3$ (Fig. 21(b)). Below this, the sharp, chard-like crystals yield a Ti-Fe-O rich chemistry (with some Ni), Figure 21(c), and probably correspond to the Fe-rich, spearhead-like crystals identified in cross-section Figure 5. EDS suggests this may be a $FeTiO_3$ illmenite phase, however only Fe_3O_4 was detected by XRD in the serial sectioning study. Finally the lower layer yields a spectrum Figure 21(d) identical to the white particles in the ledge, namely a Ni-Ti-rich oxide (with some Fe), presumably $NiTiO_3$ again.

After 800 °C oxidation, some fracture ledge features, Figure 22, are characterized by EDS as pure TiO_2 and as a Ti-Fe-Ni-rich oxide, somewhat suggestive of the Fe-rich needles discussed above. Another example of this combination is presented in Figure 23, for what appears to be a porous interface of a spalled layer. Finally, after 900 °C oxidation, some globular features revealed in fracture plateaus, Figure 24, appear to be dispersed metallic Ni particles (X) in a matrix of essentially pure TiO_2 (Y), similar to the dispersed sublayer particles in the 700 °C cross-section, Figure 5. Another area, Figure 25, indicates a dispersion of Ti-Ni-O rich particles (X), consistent with $NiTiO_3$, in a matrix of TiO_2 (Y).
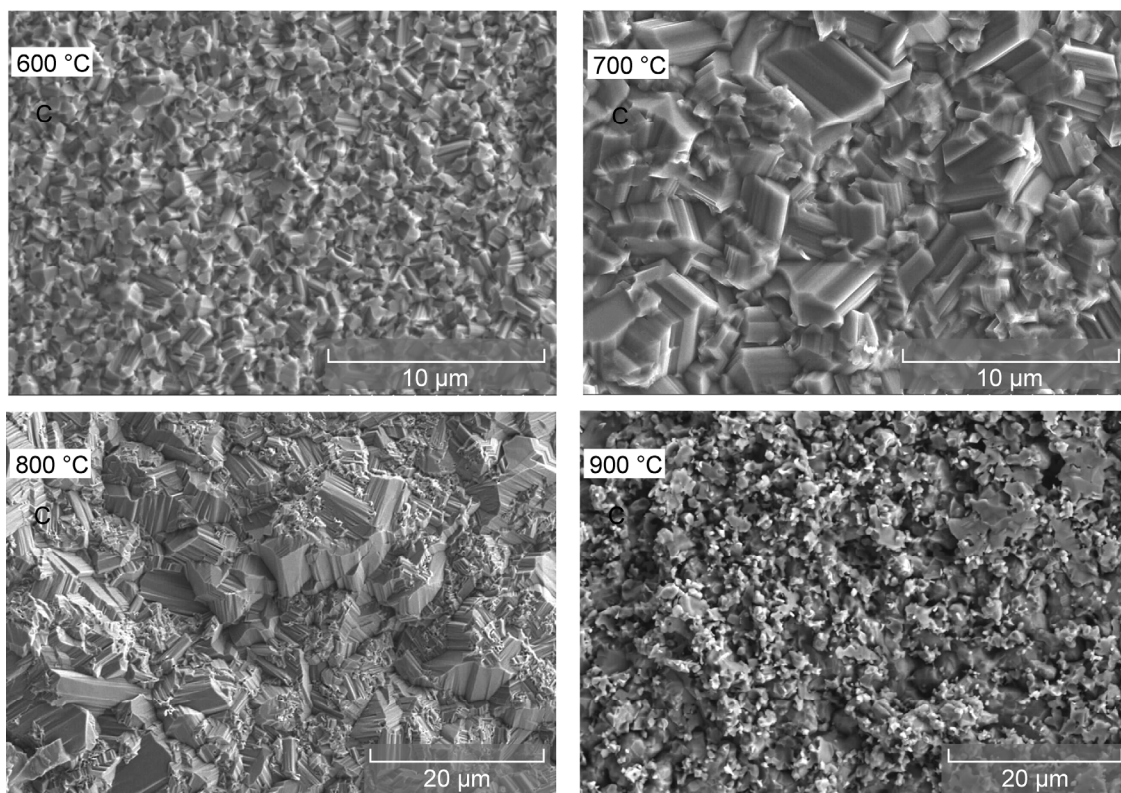
Ni49Ti

Figure 18.—Surface scale features of Ni49Ti after oxidation at 600, 700, 800, and 900 °C.
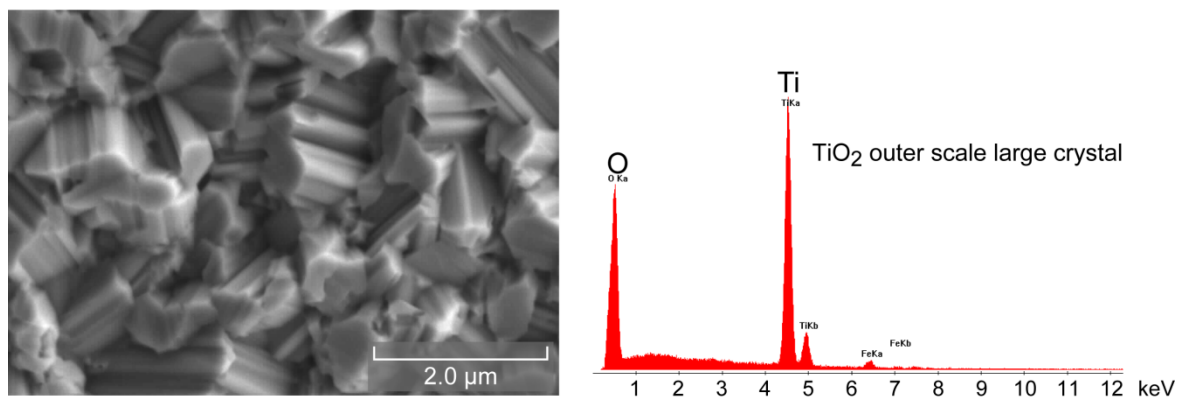
Ni49Ti 600 °C; bright, large crystals

Figure 19.—Detail of stepped facets of TiO_2 grains in the scale (Ni49Ti after 100 hr oxidation at 600 °C).
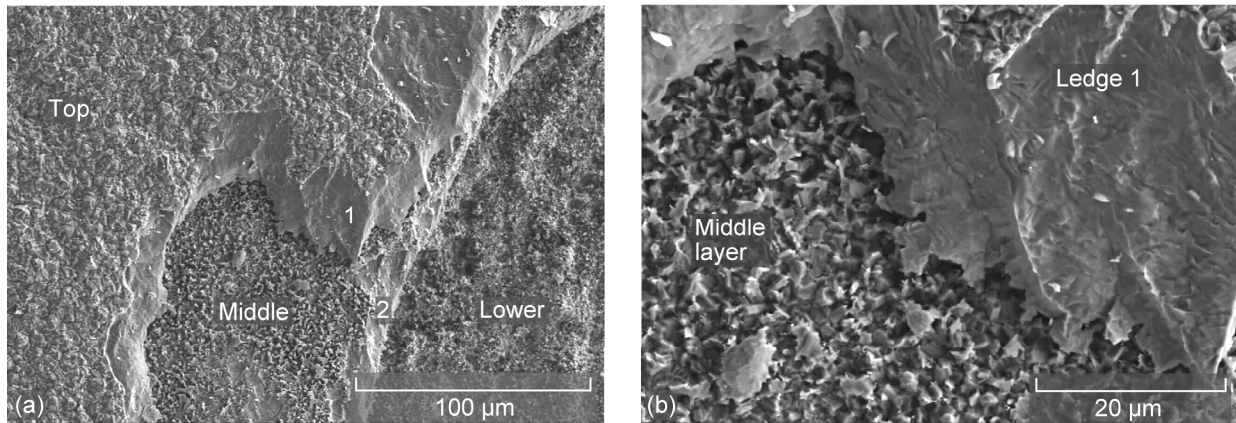
Figure 20.—Overview and detail of scalloped spall ledges in surface scale (Ni49Ti after 100 hr oxidation at 700 °C).

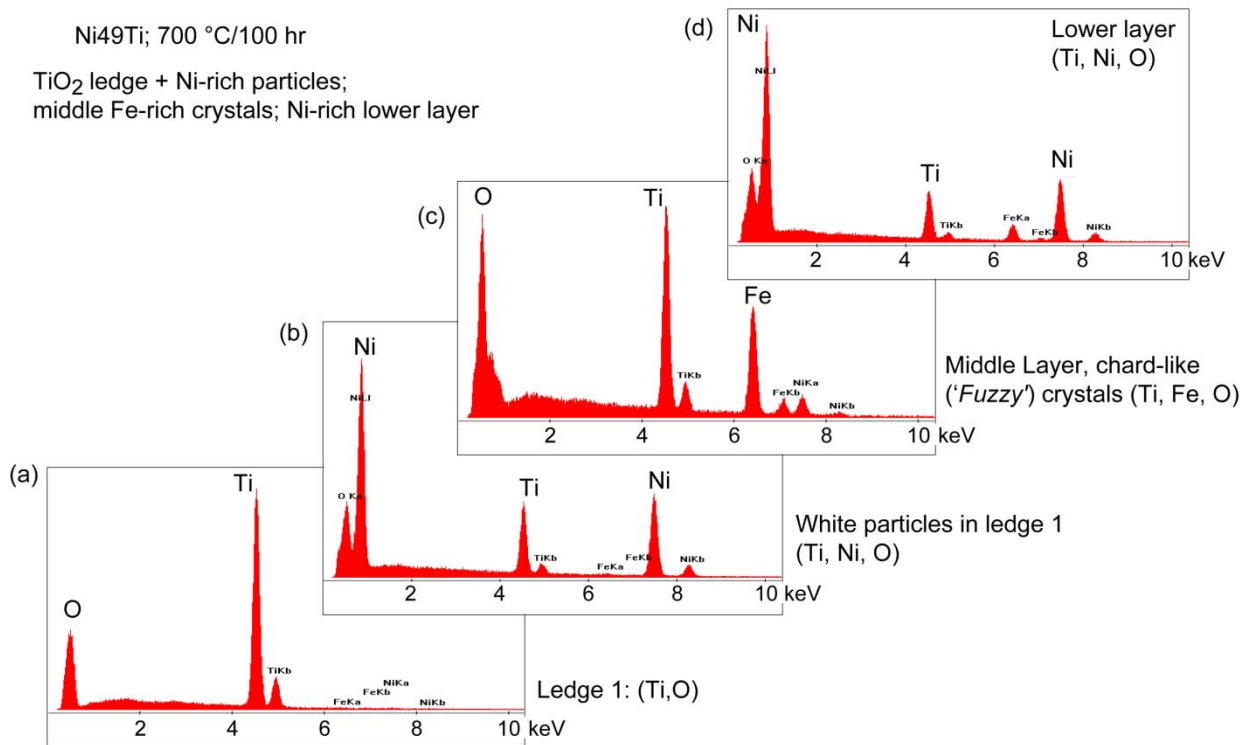Figure 21.—SEM/EDS spectra of TiO₂ surface, Ni-rich particles in fracture ledge, Fe-rich crystals in exposed middle layer, and Ni-rich innermost layer, from Figure 16.
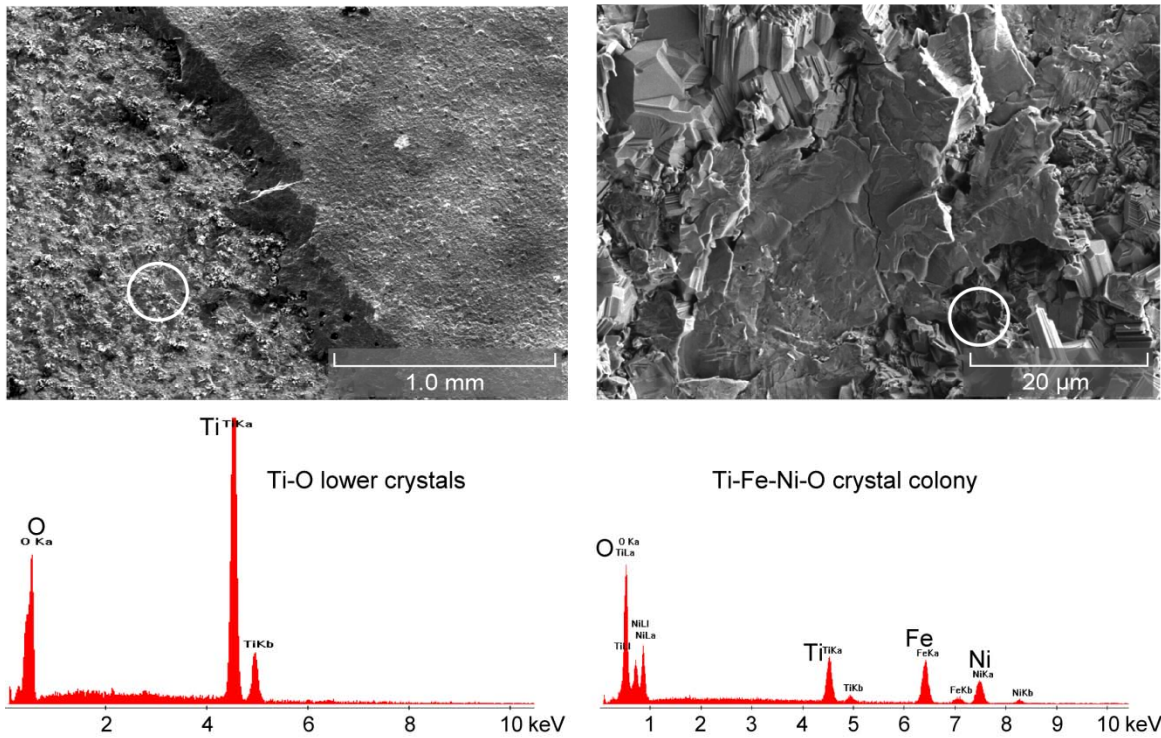
Ni49Ti: 800 °C/100 hr; scale fracture features

Ti-O lower crystals

Ti-Fe-Ni-O crystal colony

Figure 22.—Large plateaus of intact TiO_2 and spalled regions exposing Ti-Ni-Fe-rich oxide particles (Ni49Ti after 100 hr oxidation at 800 °C).

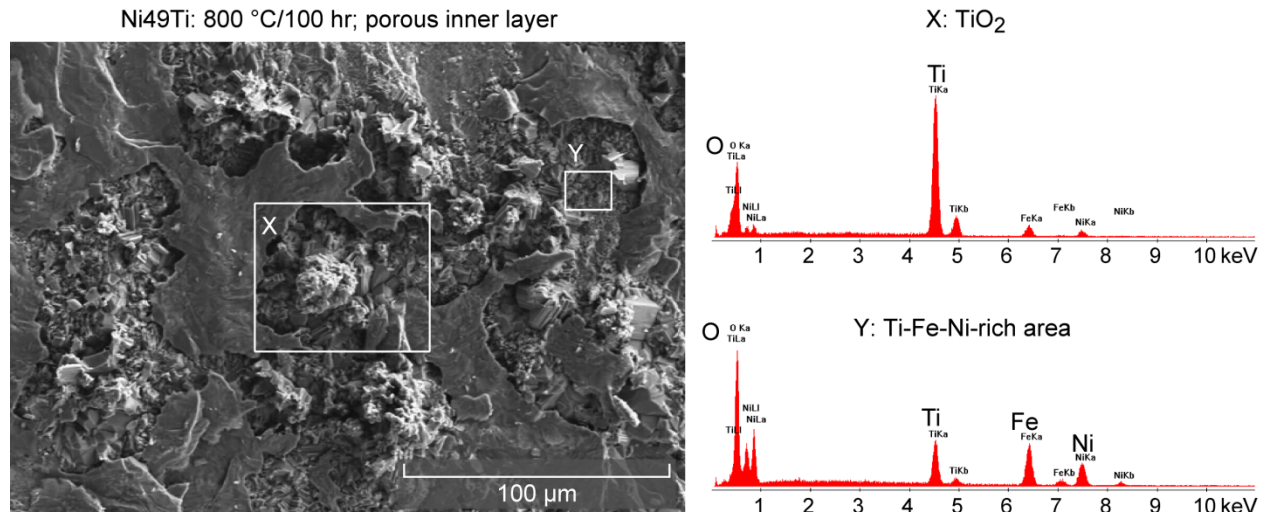Ni49Ti: 800 °C/100 hr; porous inner layer

X: TiO_2

Y: Ti-Fe-Ni-rich area

Figure 23.—Spalled regions exposing porous inner layer showing similar TiO_2 and Ti-Ni-Fe-rich oxide chemistry (Ni49Ti after 100 hr oxidation at 800 °C).
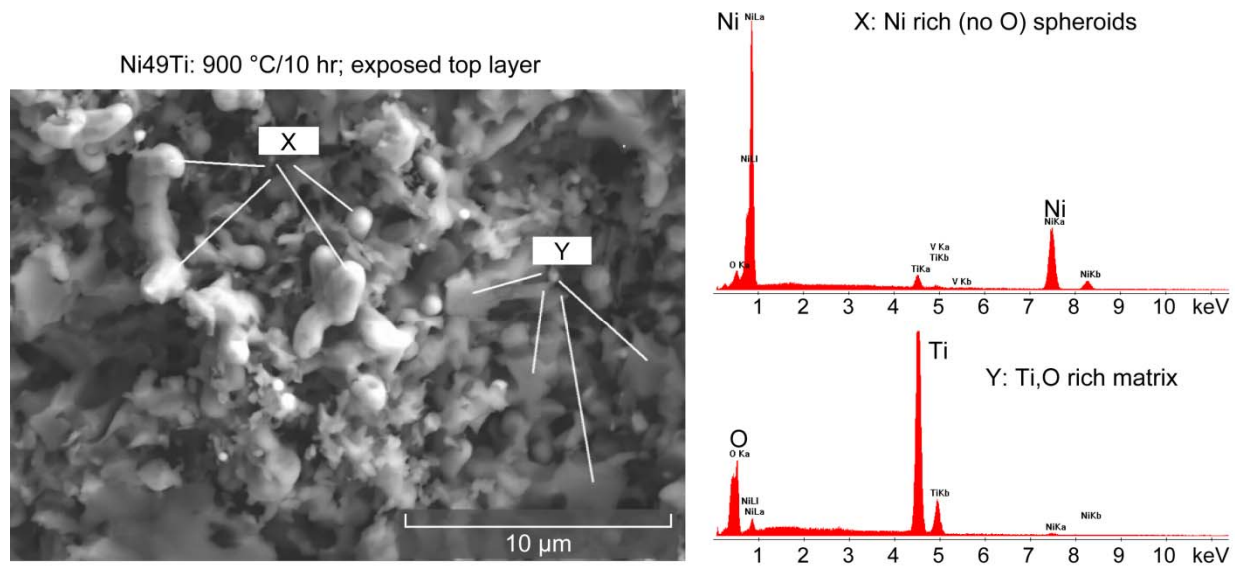
Ni49Ti: 900 °C/10 hr; exposed top layer

X: Ni rich (no O) spheroids

Y: Ti,O rich matrix

Figure 24.—Spheroidal metallic Ni particles in a TiO_2 scale matrix at the exposed outer layer (Ni49Ti after 10 hr oxidation at 900 °C).

Ni49Ti: 900 °C/10 hr; lower oxide layer
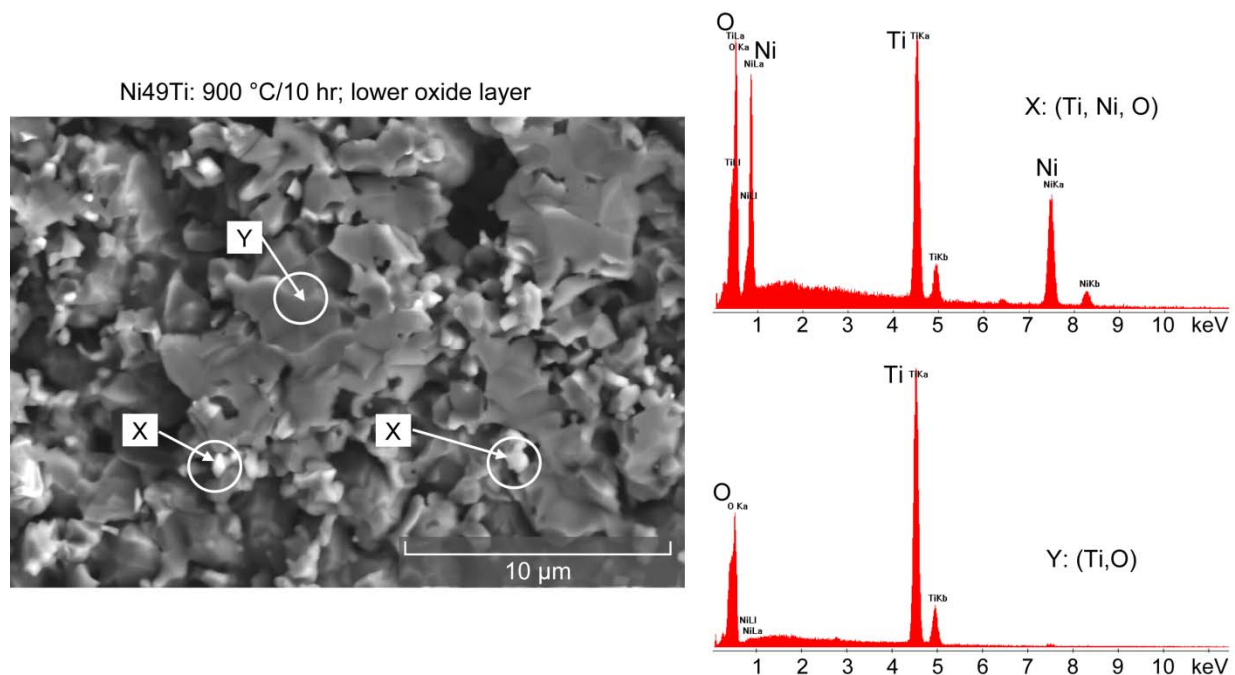
X: (Ti, Ni, O)

Y: (Ti,O)

Figure 25.—Ti-Ni-rich oxide particles in a TiO_2 scale matrix at the lower inner layer (Ni49Ti after 10 hr oxidation at 900 °C).

Ni-30Pt-50Ti

An overview for scales formed on Ni-30Pt-50Ti by oxidation at 600 to 900 °C is presented in Figure 26. Here colonies or outcroppings of the faceted and striated TiO_2 grains are seen as isolated islands on a sea of finer grain, smoother material. The progressive increase in crystal size with temperature is apparent. (However, no unspalled areas showing these features could be located for the 800 °C sample).

The structure developed at 600 °C is shown in more detail in Figure 27, and, while both the large (X) and fine grained crystals (Y) are revealed as pure TiO_2, a very fine localized dispersion of Pt(Ni)-rich spheroids (Z) was identified by the EDS spectra. At 700 °C, the large faceted crystals (X), Figure 28, are again TiO_2, but some finer grain areas (Y) yield EDS spectra most consistent with NiO, as pointed out in Figures 4 and 12. At 800 °C, multiple levels were revealed, Figure 29, and a fractured plateau reveals a distinct dispersion of bright Pt-rich particles in a matrix of TiO_2, Figure 30. This is similar to the dispersion of Pt-rich particles in the 700 °C cross-section surrounded by TiO_2. Finally, at 900 °C, Figure 31, enormous, highly-striated TiO_2 crystals are observed. Here even the fine grain external scale, Figure 31(b), appears highly crystallographic and faceted. Lower layers, exposed by spallation, show both cleaved, flat grains (Fig. 32(a)) and filamentary or needle-like features, clustered in parallel colonies (Fig. 32(b)). Both regions of the lower layers are peppered with a fine dispersion of bright particles, presumably Pt-rich metal again. All these regions produced EDS spectra consistent with TiO_2 as the primary phase, Figure 33.
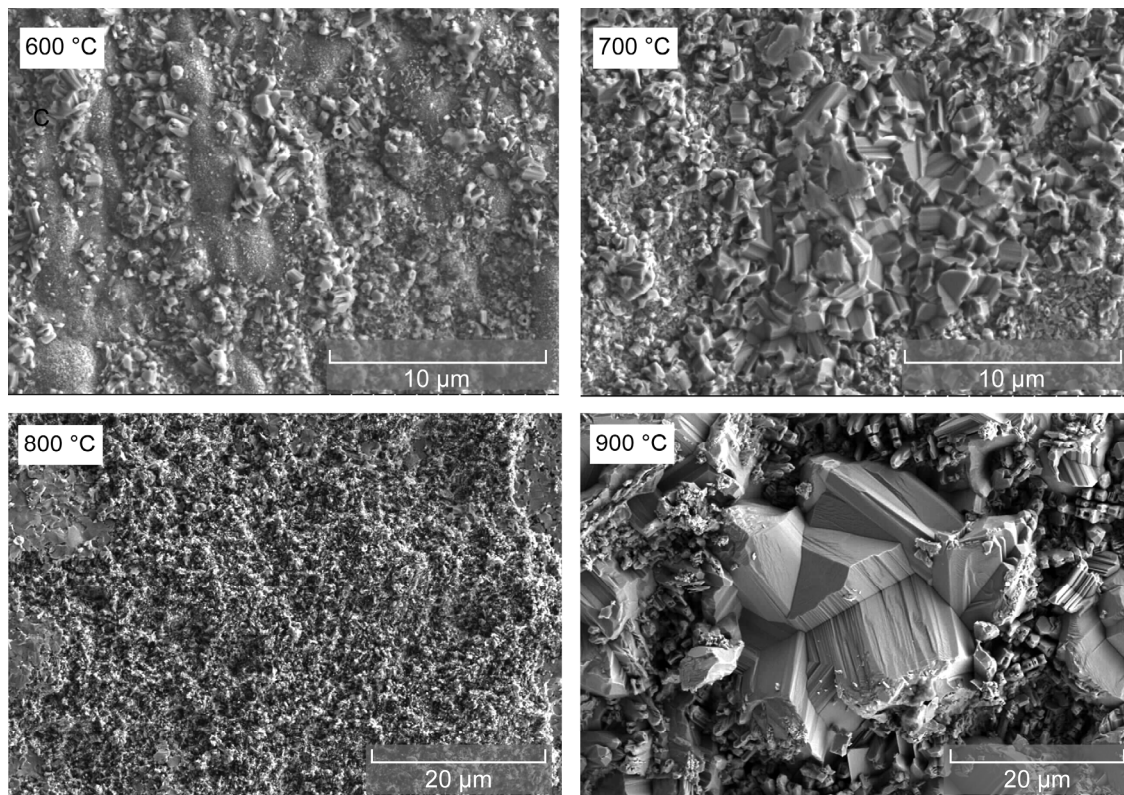

Figure 26.—Duplex grain structure in outer scale layers for Ni30Pt50Ti after oxidation at 600, 700, 800, and 900 °C.

Ni30Pt50Ti; 600 °C
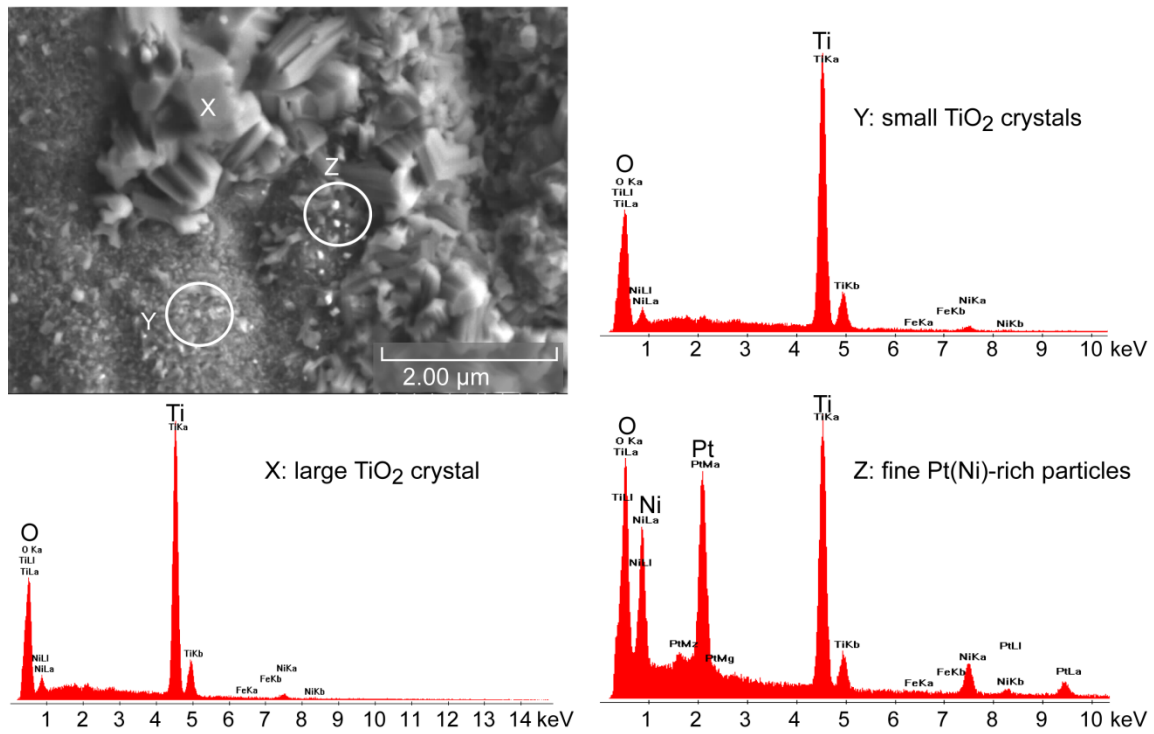Duplex terrain: Ti-O fine grain plateau with Pt,Ni-rich particles; coarser Ti-O crystals colonies

Figure 27.—Coarser faceted and fine grain TiO_2 crystals and Pt(Ni)-rich particles on the surface of oxidized Ni30Pt50Ti after 100 hr oxidation at 600 °C.

Ni30Pt50Ti; 700 °C
Duplex terrain: fine grain plateau,
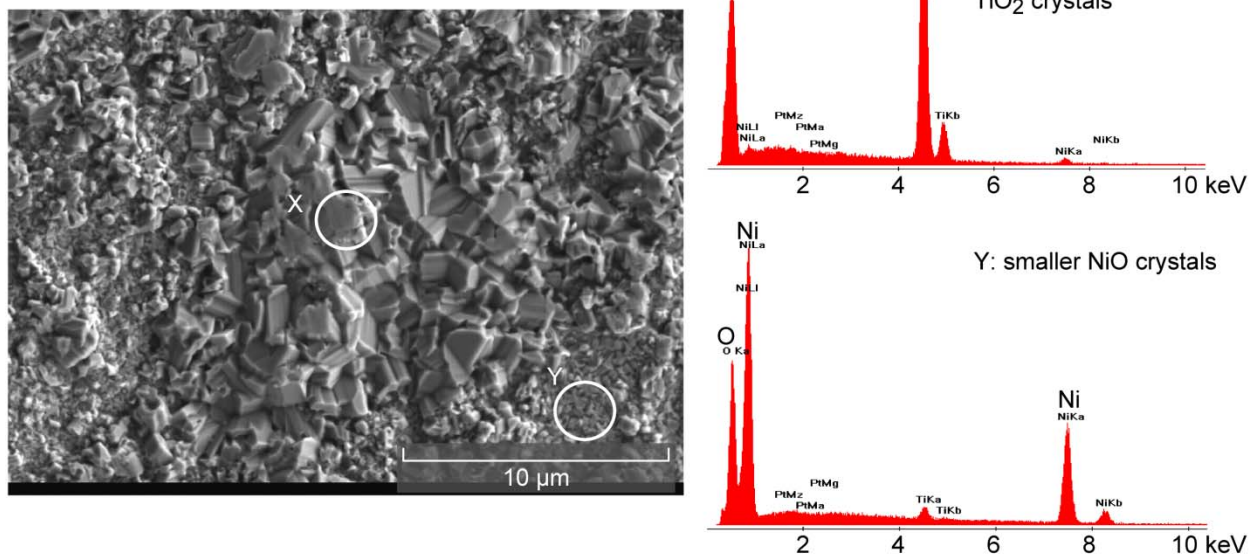coarse crystals colonies and Pt particles

Figure 28.—Duplex grain structure and fine grain Ni-rich oxide on oxidized Ni30Pt50Ti after 100 hr oxidation at 700 °C.
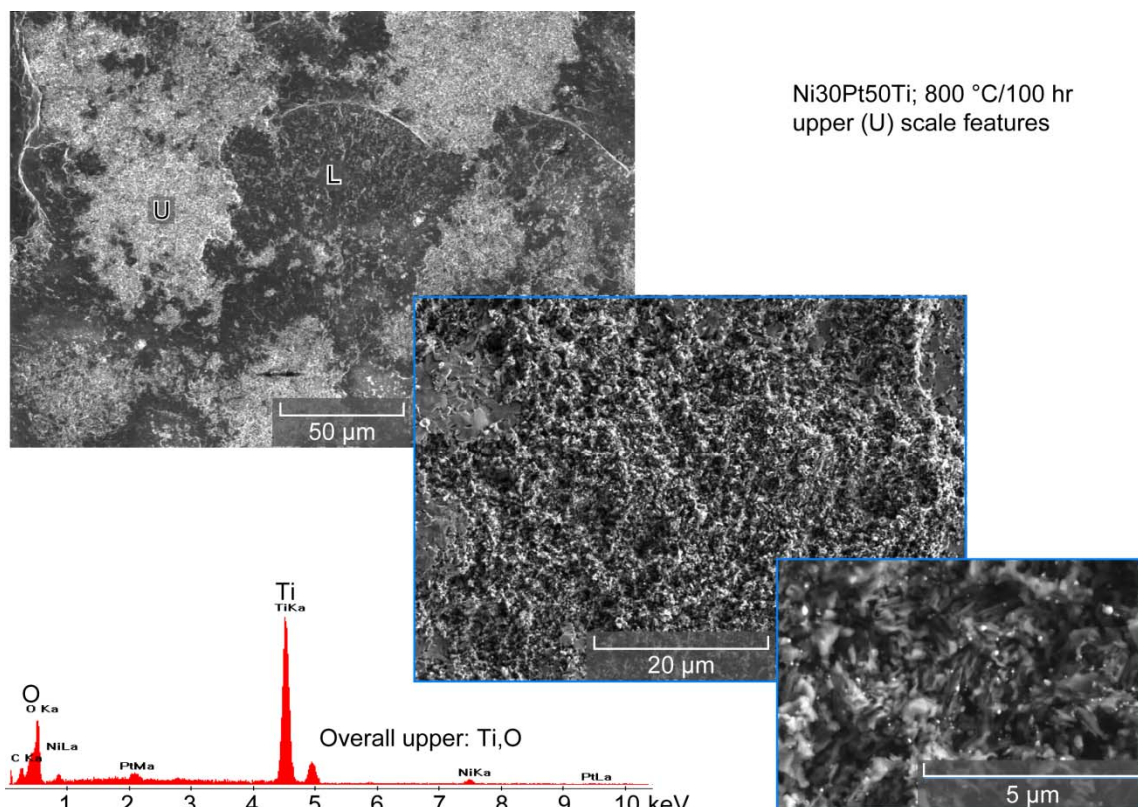
Ni30Pt50Ti; 800 °C/100 hr
upper (U) scale features

50 μm

20 μm

5 μm

Ti
TiKa

O
O Ka

C Ka

NiLa

PtMa

NiKa

PtLa

Overall upper: Ti,O

1   2   3   4   5   6   7   8   9   10 keV

Figure 29.—Large plateaus of spalled regions and structures at various levels of detail for spalled upper surface of TiO_2 scale (Ni30Pt50Ti after 100 hr oxidation at 800 °C).

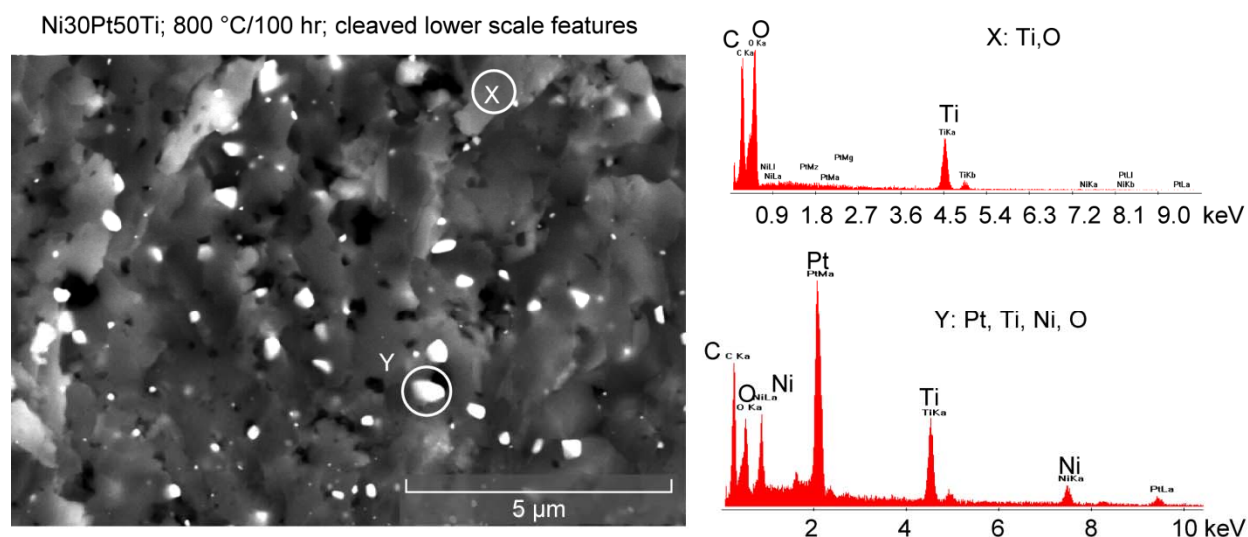Ni30Pt50Ti; 800 °C/100 hr; cleaved lower scale features

X: Ti,O

C
C Ka

O
O Ka

NiLi
NiLa

PtMz
PtMa

PtMg

Ti
TiKa

TiKb

NiKa

PtLi
NiKb

PtLa

0.9 1.8 2.7 3.6 4.5 5.4 6.3 7.2 8.1 9.0 keV

5 μm

Y: Pt, Ti, Ni, O

Pt
PtMa

C
C Ka

O
O Ka

NiLn

Ni

Ti
TiKa

Ni
NiKa

PtLa

2   4   6   8   10 keV

Figure 30.—Cleaved plane in lower scale showing TiO_2 matrix with Pt-Ni-rich particles (Ni30Pt50Ti after 100 hr oxidation at 800 °C).
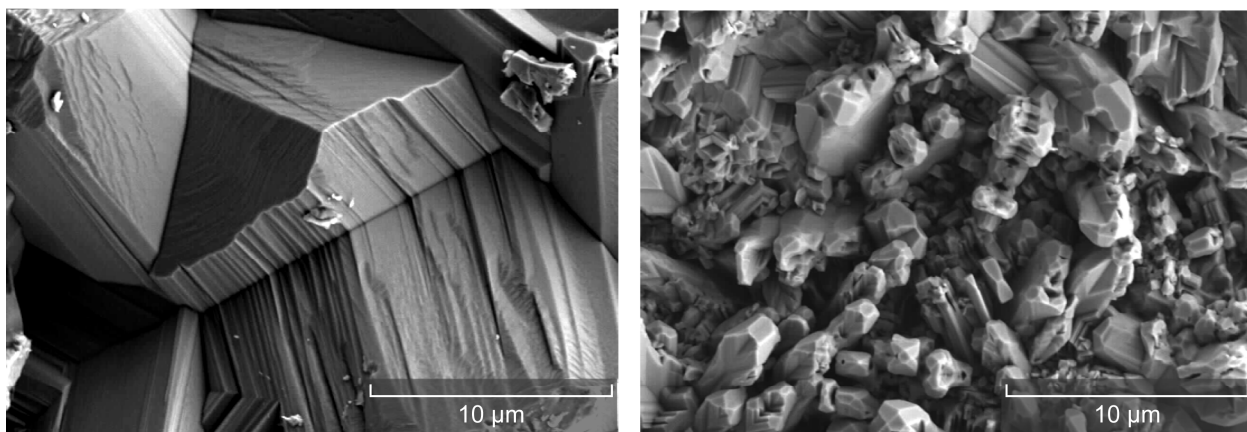
Figure 31.—Highly striated massive crystals and crystallographically faceted fine grain structures (Ni30Pt50Ti after 10 hr oxidation at 900 °C).
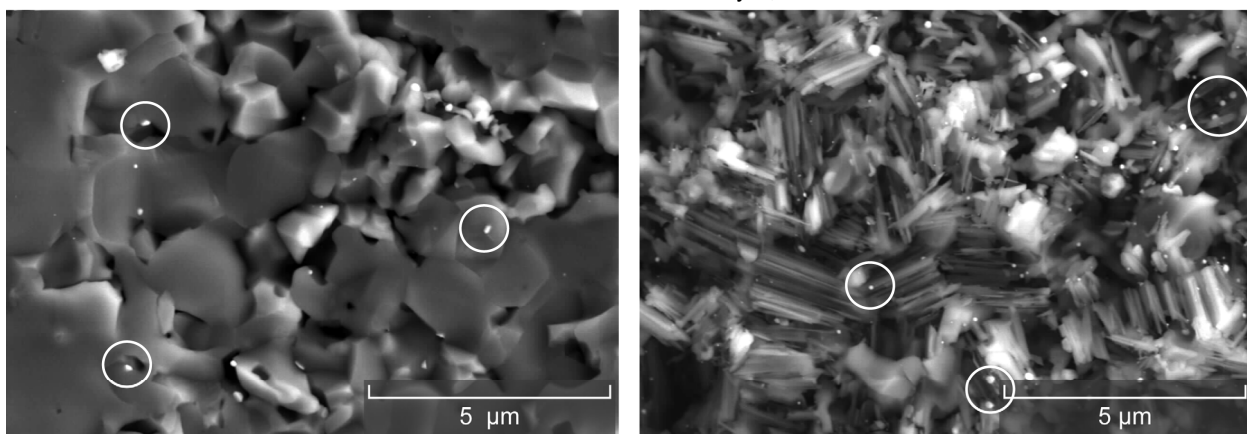
Ni30Pt50Ti: 900 °C/lower layer; 10 hr

Figure 32.—Cleaved and striated fibrous grains and fine spheroidal particles in spalled region of scale formed on Ni30Pt50Ti after 10 hr oxidation at 900 °C.
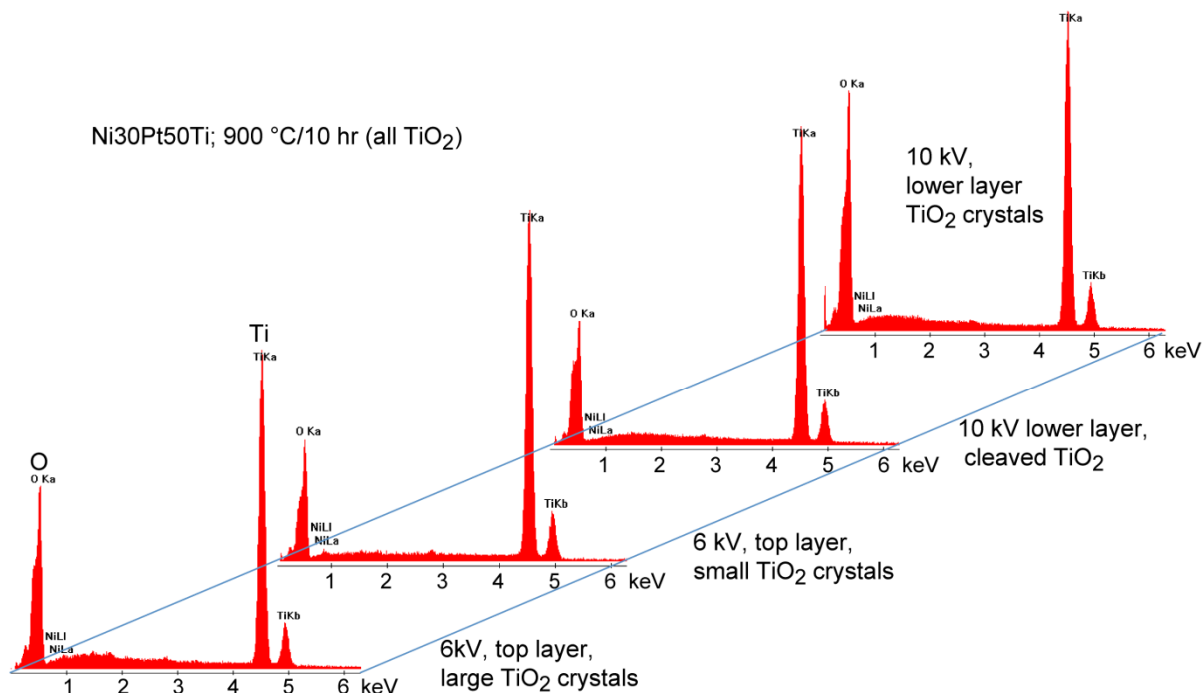
Figure 33.—SEM/EDS spectra showing similar Ti-O profiles for outer large or fine grain scales and lower cleaved or striated grains (Ni30Pt50Ti after 10 hr oxidation at 900 °C).

Discussion

The above confirms that a commercial NiTi and an experimental Ni(Pt)Ti shape memory alloy form primarily fast-growing TiO_2 rutile scales over a wide temperature range and after relatively long-term exposure. Thus the report of activation energies (250 kJ/mole K) near that reported for other Ni-Ti studies exhibiting rutile as the primary scale phase is not unexpected. The TiO_2 anatase phase may have been present as a trace for the NiTi alloy at low temperature. $NiTiO_3$ formed as secondary oxides on both alloys, reaching a maximum on the order of 25 percent. This oxide phase was difficult to distinguish microstructurally in cross-section and often appeared as small dispersed particles in plan SEM. NiO was also somewhat elusive microstructually. As demonstrated by serial and taper-section XRD and by SEM in plan and cross-sections, it was present only as a minor phase <20 percent, appeared to predominate at the gas surface and only for the NiPtTi alloy. Proceeding inward, dispersed metallic Ni(Ti) and Pt(Ni) solid solution particles were observed on the NiTi and NiPtTi alloys, respectively. Finally, metallic depletion zones are encountered, first as fingerlike protrusions into the scale, then as a continuous layer of predominantly Ni_3Ti or Pt_3Ti, with some oxygen in solid solution. The NiPtTi substrate also appeared to have thermally-aged into a mixture of the B19 Pt(Ni)Ti martensitic phase and a new hexagonal structure of similar composition, perhaps a new martensitic variant or grain boundary-decomposition phase. The Fe_3O_4 and TiC were identified as artifacts from unintentional processing impurities, such as melting in graphite crucibles, and are believed to have been relatively innocuous to the primary oxidation process.

Most of the scale features identified on the NiTi alloy have been observed to various degrees and under various conditions in the literature. The serial-sectioning XRD study by Satow et al. (Ref. 2) catalogued the transition from a pure rutile external scale, to a mixture with $NiTiO_3$, to a Ni then Ni_3Ti depletion zone, and finally the NiTi substrate. Others observed the anatase structure sporadically, primarily for lower temperature and shorter time exposures. Porosity was more prevalent in some studies, and spalling was occasionally observed. Dispersed metallic particles and depletion zones sometimes took the form of various Ni_xTi_y stoichiometry. A NiPdTi alloy exhibited some reduction in growth rate as did the NiPtTi here.

It has been mentioned that the NiPtTi ternary alloy oxidized with parabolic kinetics about four times lower than that of the binary NiTi alloy. Since the oxide phases were quite similar on both alloys, the difference cannot be explained by modifications in the scale growth and diffusivity. However the existence of a continuous Pt_3Ti depletion zone may serve to restrict Ti outward diffusion from the substrate, as compared to an Ni_3Ti zone for the binary alloy. Associated with this feature, the dispersion of metallic particles in the scale appear as solvent remnants from the oxidation of Ti "solute" constituent. In the case of the NiTi binary, this phase appears as a fine dispersion in the inner layer of a duplex TiO_2 scale, trending toward the Ni_3Ti metallic fingers and the depeletion zone. For the NiPtTi alloy, a 13-μm mixed cermet zone of $Pt(Ni) + TiO_2$ inner scale trended toward Pt_3Ti fingers and depletion zone. The noble inert Pt phase can thus be viewed as a partial diffusion barrier retarding the outward transport of Ti toward the oxidative interface (or retarding the inward transport of oxygen).

One of the more unusual features of these scales is the presence of dispersed, unoxidized Ni particles embedded in a TiO_2 matrix. These presumably were metallic remnants of the NiTi substrate after the Ti was completely depleted by selective oxidation. The fact that they were not oxidized perhaps indicates that the local pO_2 is below that needed to oxidize Ni. Another possibility is that the growth of TiO_2 is very rapid in comparison to NiO growth (about 10x on average k_p increase (Ref. 2)). Thus, Ti is extracted out of the alloy, leaving Ni in a metastable metallic state, only gradually being converted to $NiTiO_3$. The fact that relatively little $NiTiO_3$ and metallic Ni are found in the scale suggests that the primary steady state growth mechanism is outward transport of Ti, leaving Ni-rich phases behind as depleted layers. However the concentration of $NiTiO_3$ in the outer layers suggests an initial transient oxidation product and inward new growth by oxygen diffusion. Internal oxidation and breakup of the metallic diffusion zone found in more dilute alloys is similar to the finger structure of the depletion zones here and the isolation of individual particles in the scale. Since Ti is well known for its affinity for oxygen in solution, it is not surprising to find some manifestation of its internal oxidation tendencies here.

It is also interesting to compare the above features to those observed for Ni-5,10,15Ti alloys (Ref. 14). Here more distinct layers were formed, with NiO at the gas surface, followed by an $NiTiO_3$ layer, then internal fingers of TiO_2. Ti-depletion zones were formed beneath the scale similar to the NiTi SMAs. The kinetics were analyzed to be somewhat between those of pure Ni and NiTi SMA alloys (Ref. 2).

Given the rich, detailed structures described above, perhaps the most obvious structural feature is the most striking, that of striated, faceted external TiO_2 crystals. These are seen to enlarge quite dramatically with oxidation temperature. Such external growth features suggest some component of outward Ti diffusion. A summary figure of the average crystal width is given in Figure 34, suggesting a type of Arrhenius relation based on a thermally-activated process. Note that the scale grains are approximately equal for both Ni49Ti and Ni-30Pt-50Ti alloys, even though the scale thickness growth rates were faster for the binary alloy. Also, note that the ternary alloy possessed a more prominent fine-grain base scale (dashed curve) that was approximately seven times smaller than the larger grain outcroppings.

This figure also compares the grain size found for TiO_2 scales on other NiTi and Ti alloys. Again, Arrhenius-type relations are suggested, but for considerably smaller sizes. This difference is primarily due to the long times used here (100 hr) compared to those in the literature (4 hr, Vojtêch et al. and Xu et al. (Refs. 8 and 9); 1 to 2 hr, Park (Ref. 15)). Vojtech et al. attempted to determine an activation energy by estimating scale growth kinetic constants, albeit from limited time data, assuming a $t^{1/3}$ kinetic law. They determined that to be 45 kJ/mole, or about 1/3 that of the oxidation kinetics, as reflected in the shallow slope of their curve in Figure 34. No kinetic grain growth rates were determined in the present study.
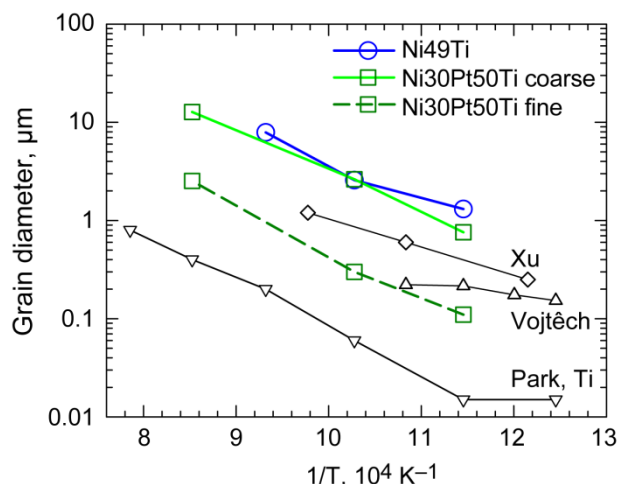
Figure 34.—Temperature effects on increased grain size: TiO$_2$ scales formed in this study compared to literature values (Refs. 7, 8, and 15).

Summary

Ni49Ti and Ni-30Pt-50Ti shape memory alloys have been isothermally-oxidized in air at 500 to 900 °C. The scales were characterized by SEM/EDS and XRD in plan, cross-section, and serial or tapered sections. TiO$_2$ rutile phases dominated the scale make-up, with distinct striated and faceted external grain structure. The grain size was found to be highly temperature dependent and similar for each alloy, but more uniform on the binary alloy and duplex on the ternary. The NiPtTi alloy exhibited many features in common with the NiTi alloy, but at about 1/2 the overall scale thickness, as expected from the previous thermogravimetric kinetic study. NiTiO$_3$ was also found, primarily for NiPtTi and in outer layers of the scale, but in amounts less than that expected for complete alloy oxidation. The excess Ni appeared to concentrate in dispersed metallic particles or in the Ni$_3$Ti and (Pt,Ni)$_3$Ti depletion zones. It is believed that the dispersed Pt(Ni,Ti) particulate and continuous (Pt,Ni)$_3$Ti depletion zone contributes to a reduced oxidation rate by limiting outward diffusion of Ti compared to alloys without Pt. In addition, a previously unreported hexagonal phase with the Ni$_3$Sn structure (D0$_{19}$) was observed in the Ni-30Pt-50Ti samples oxidized (aged) at 700 °C.

References

1. R. Noebe, D. Gaydosh, S. Padula, A. Garg, T. Biles, and M. Nathal, "Properties and Potential of Two (Ni,Pt)Ti Alloys for Use as High-Temperature Actuator Materials," in Smart Structures and Materials 2005: Active Materials: Behavior and Mechanics, SPIE Conf. Proc. vol. 5761, (2005), pp. 364–375.
2. J.L. Smialek, D.L. Humphrey, and R.D. Noebe, "Comparative Oxidation Kinetics of a High Temperature NiPtTi Shape Memory Alloy," Oxidation of Metals, 74, No. 3 (2010), pp. 125–144.
3. T. Satow, T. Isano, and T. Honma, "The High Temperature Oxidation of Intermetallic Compound NiTi," Journal of the Japan Institute of Metals, 38 (1974) 242–246.
4. C.M. Chan, S. Trigwell, T.W. Duerig, "Oxidation of an NiTi Alloy," Surface and Interface Analysis, 5, pp. 349–354 (1990).
5. C.L. Chu, S.K. Wu, Y.C. Yen, "Oxidation behavior of equiatomic TiNi alloy in high temperature air environment," Materials Science and Engineering, A 216, pp. 193–200 (1996).
6. G.S. Firstov, et al., "Surface oxidation of NiTi shape memory alloy," Biomaterials, 23, pp. 4863–4871 (2002).

7. L. Zhu, J.M. Fino, and A. Pelton, "Oxidation of Nitinol," in SMST–2003, Proceedings of the International Conference on Shape Memory and Superplastic Technologies, eds. T.W. Duerig and A. Pelton, SMST–ASM International, Metals Park, OH (2003).
8. D. Vojtěch, P. Novák, M. Novák, L. Jaska, T. Fabián, J. Maixner, and V. Machovič, "Cyclic and isothermal oxidation of nitinol wire at moderate temperatures," Intermetallics, 16 (2008) 424–431.
9. C.H. Xu, X.Q. Ma, S.Q. Shi, C.H. Woo, "Oxidation behavior of TiNi shape memory alloy at 450–750 °C," Materials Science and Engineering, A 371, pp. 45–50 (2004).
10. Q. Tian and J. Wu, "Effect of the Rare Earth Element Ce on Oxidation Behavior of TiPdNi Alloys," Materials Science Forum, 394–395, pp. 455–458 (2002).
11. Q. Tian, J. Chen, Y. Chen, and J. Wu, "Oxidation behavior of TiNi-Pd shape memory alloys," Z. Metallkde., 94, pp. 36–40 (2003).
12. K-N. Lin and S-K Wu, "Oxidation Behavior of Ti50Ni40Cu10 Shape-Memory Alloy in 700–1000 °C Air," Oxidation of Metals, 71 (2009) 187–200.
13. J.L. Smialek, D.L. Humphrey, and R.D. Noebe, "Oxidation Kinetics of a NiPtTi High Temperature Shape Memory Alloy," NASA/TM—2007-214697, NASA, Washington, DC.
14. C.L. Zeng, M.C. Li, G.Q. Liu, and W.T. Wu, "Air Oxidation of Ni-Ti Alloys at 650–850 °C," Oxidation of Metals, 58 (2002) 171-184.
15. Y-J. Park, H-J. Song, I. Kim, H-S. Yang, "Surface characteristics and bioactivity of oxide film on titanium metal formed by thermal oxidation," J. Mater. Med., 18 (2007) 565–575.

Bibliography

Atkinson, A.; Taylor R.I.; and Hughes A.E. (1982): A Quantitative Demonstration of the Grain Boundary Diffusion Mechanism for the Oxidation of Metals. Phil. Mag., vol. A45, pp. 823–833.

DeCastro, J.A.; Melcher, K.J.; and Noebe, R.D. (2005): System-Level Design of a Shape Memory Alloy Actuator for Active Clearance Control in the High-Pressure Turbine. AIAA–2005–3988.

Gulbransen, E.A.; and Andrew, K.F. (1954): The Kinetics of Oxidation of High Purity Nickel. J. Electrochem. Soc., vol. 128, pp. 121–140.

Kofstad, P. (1988): High Temperature Corrosion. Elsevier Applied Science, London, pp. 212 and 293.

Lindquist, P.G.; and Wayman C.M. (1990): Shape Memory and Transformation Behavior of Martensitic Ti-Pd-Ni and Ti-Pt-Ni Alloys. Engineering Aspects of Shape-Memory Alloys, T.W. Duerig et al., eds., Butterworth-Heinemann, London, pp. 58–68.

Noebe, R.D.; Biles, T.; and Padula, S.A. (2006): Chapter 7: NiTi-Based High-Temperature Shape-Memory Alloys: Properties, Prospects, and Potential Applications. Advanced Structural Materials: Properties, Design Optimization, and Applications, W.O. Soboyejo, ed., Taylor & Francis Group, Boca Raton, FL, pp. 141–180.

Noebe, R., et al. (2006): Effect of Thermomechanical Processing on the Microstructure, Properties, and Work Behavior of a $Ti_{50.5}Ni_{29.5}Pt_{20}$ High-Temperature Shape Memory Alloy. SMST 2006: Proceedings of the International Conference on Shape Memory and Superelastic Technologies, ASM International, Metals Park, OH, pp. 409–426.

Otsuka, K.; and Wayman, C.M., eds. (1998): Shape Memory Materials. Cambridge University Press, Cambridge, U.K.

Pieraggi, B. (1987): Calculations of Parabolic Reaction Rate Constants. Oxid. Met., vol. 27, pp. 177–185.

Progar, D.J.; and Lewis, B.W.: A Study of Oxidation Kinetics of Nickel Metal in Flowing Air and Oxygen-Nitrogen Mixtures. NASA TN–D–2224, 1964.

Rios, O., et al. (2005): Characterization of Ternary NiTiPt High-Temperature Shape Memory Alloys. Smart Structures and Materials 2005: Active Materials: Behavior and Mechanics, SPIE Conference Proceedings, vol. 5761, pp. 376–387.

Smialek, J.L.; and Humphrey, D.L. (1992): Oxidation Kinetics of Cast $TiAl_3$. Scripta Metall. Mater., vol. 26, pp. 1763–1768.

1. REPORT DATE (DD-MM-YYYY) 01-09-2011	2. REPORT TYPE Technical Memorandum	3. DATES COVERED (From - To)

4. TITLE AND SUBTITLE
Oxide Scales Formed on NiTi and NiPtTi Shape Memory Alloys

5a. CONTRACT NUMBER

5b. GRANT NUMBER

5c. PROGRAM ELEMENT NUMBER

6. AUTHOR(S)
Smialek, James, L.; Garg, Anita; Rogers, Richard, B.; Noebe, Ronald, D.

5d. PROJECT NUMBER

5e. TASK NUMBER

5f. WORK UNIT NUMBER
WBS 984754.02.07.03.16.04

7. PERFORMING ORGANIZATION NAME(S) AND ADDRESS(ES)
National Aeronautics and Space Administration
John H. Glenn Research Center at Lewis Field
Cleveland, Ohio 44135-3191

8. PERFORMING ORGANIZATION REPORT NUMBER
E-17748

9. SPONSORING/MONITORING AGENCY NAME(S) AND ADDRESS(ES)
National Aeronautics and Space Administration
Washington, DC 20546-0001

10. SPONSORING/MONITOR'S ACRONYM(S)
NASA

11. SPONSORING/MONITORING REPORT NUMBER
NASA/TM-2011-217096

12. DISTRIBUTION/AVAILABILITY STATEMENT
Unclassified-Unlimited
Subject Category: 26
Available electronically at http://www.sti.nasa.gov
This publication is available from the NASA Center for AeroSpace Information, 443-757-5802

13. SUPPLEMENTARY NOTES

14. ABSTRACT
Ni-49Ti and Ni-30Pt-50Ti (at.%) shape memory alloys were oxidized isothermally in air over the temperature range of 500 to 900 °C. The microstructure, composition, and phase content of the scales were studied by SEM, EDS, XRD, and metallography. Extensive plan view SEM/EDS identified various features of intact or spalled scale surfaces. The outer surface of the scale was a relatively pure TiO_2 rutile structure, typified by a distinct highly striated and faceted crystal morphology. Crystal size increased significantly with temperature. Spalled regions exhibited some porosity and less distinct features. More detailed information was obtained by correlation of SEM/EDS studies of 700 °C/100 hr cross-sections with XRD analyses of serial or taper-polishing of plan surfaces. Overall, multiple layers exhibited graded mixtures of NiO, TiO_2, $NiTiO_3$, Ni(Ti) or Pt(Ni,Ti) metal dispersoids, Ni_3Ti or Pt_3Ti depletion zones, and substrate, in that order. The NiTi alloy contained a 3 at.% Fe impurity that appeared in embedded localized Fe-Ti-rich oxides, while the NiPtTi alloy contained a 2 v/o dispersion of TiC that appeared in lower layers. The oxidation kinetics of both alloys (in a previous report) indicated parabolic growth and an activation energy (250 kJ/mole) near those reported in other Ti and NiTi studies. This is generally consistent with TiO_2 existing as the primary scale constituent, as described here.

15. SUBJECT TERMS
Nitinol alloys; Oxidation; Scale (corrosion)

16. SECURITY CLASSIFICATION OF:			17. LIMITATION OF ABSTRACT	18. NUMBER OF PAGES	19a. NAME OF RESPONSIBLE PERSON STI Help Desk (email:help@sti.nasa.gov)
a. REPORT U	b. ABSTRACT U	c. THIS PAGE U	UU	36	19b. TELEPHONE NUMBER (include area code) 443-757-5802